6-2014

Earthquake Relocation and Focal Mechanism Analysis in the Area of Rupture Following the Mw = 7.6 September 5 2012 Nicoya Earthquake Costa Rica

Gregory Brenn
Union College - Schenectady, NY

Earthquake Relocation and Focal Mechanism Analysis in the Area of Rupture Following the M_w = 7.6 September 5, 2012 Nicoya Earthquake, Costa Rica

By

Gregory Randall Brenn

****

Submitted in partial fulfillment of the requirements for Honors in the Department of Geology

UNION COLLEGE

June, 2014

ACKNOWLEDGEMENTS

I would first like to thank my on-campus advisor, Prof. Matthew Manon, for providing both support and guidance throughout this research experience. I would also like to thank Dr. Marino Protti for educating the KECK group in seismology field methods, aiding in the deployment of the seismic network, and being patient with my incessant questions about Nicoya Peninsula seismology. A special thanks goes to Deborah Klein for always lending a hand around the Union geology department. Lastly, I would like to thank my parents for constantly supporting me in my endeavors throughout my time at Union, no matter how far-fetched those adventures may be.

TABLE OF CONTENTS

LIST OF FIGURES

ABSTRACT

As part of a Keck Geology Consortium project on the Nicoya Peninsula, Costa Rica, a dense broadband seismic array was installed directly above the rupture zone of the long-anticipated Nicoya September 5th, 2012, Mw= 7.6 earthquake. 5 Nanometrics Trillium compact seismometers and Taurus digitizers were installed, defining a ~200km triangular area with one triangular side oriented parallel to the trench and the apex located ~15km inland from the coast. This seismic network was operating from July 2nd to July 18th, and with this data combined with the permanent stations of the Nicoya broadband network, 254 events were initially located. Comparison of velocity models and Vp/Vs ratios was performed to reduce the amount error between the calculated travel times versus the expected travel times of each event. On June 23rd, a Mw= 5.7 aftershock was recorded in the area of rupture of the September 5th event, the largest event to hit the Peninsula during data collection. The aftershocks of this Mw= 5.7 event on June 23 and June 24 were located at depths of 20.9 ± 5.7 km, along the plate interface beneath the Nicoya Peninsula. This event ruptured an area of the plate interface that did not fully rupture during the September 5th event. Analysis of focal mechanisms for individual interplate events indicates dominant thrust faulting motion, consistent with underthrusting along the seismogenic zone, and combined focal mechanisms provide accurate evidence of normal fault motion. The normal faulting earthquakes most likely formed from extension at the outer rise, which were then subducted and reactivated by dehydration reactions beneath the Nicoya Peninsula. This study, combined with previous and future seismic studies, has allowed for a better understanding of where seismogenic zone earthquakes occur beneath the Nicoya Peninsula following a large magnitude event, exemplifying the benefit of dense local seismic networks to monitor for smaller magnitude seismicity that otherwise would have gone unnoticed.

INTRODUCTION

Subduction zones generate ~90% of the Earth's seismic energy (Pacheco et al., 1992). Since most of the world's largest earthquakes are located along these subduction boundaries, it is extremely important to study and understand the geological processes that create this seismicity, as megathrust earthquakes pose significant risks for those living in densely populated coastal areas. The Nicoya Peninsula, Costa Rica, represents an ideal location to study earthquake seismicity in a subduction zone environment, because it lies directly above the seismically active plate interface with its coastline only 60 km east of the Middle America Trench (Figure 1). Due to the peninsula's proximity to the trench, the seismogenic zone, the part of the subducting plate interface that produces earthquakes due to stick-slip sliding (Dixon et al., 2009) is located directly

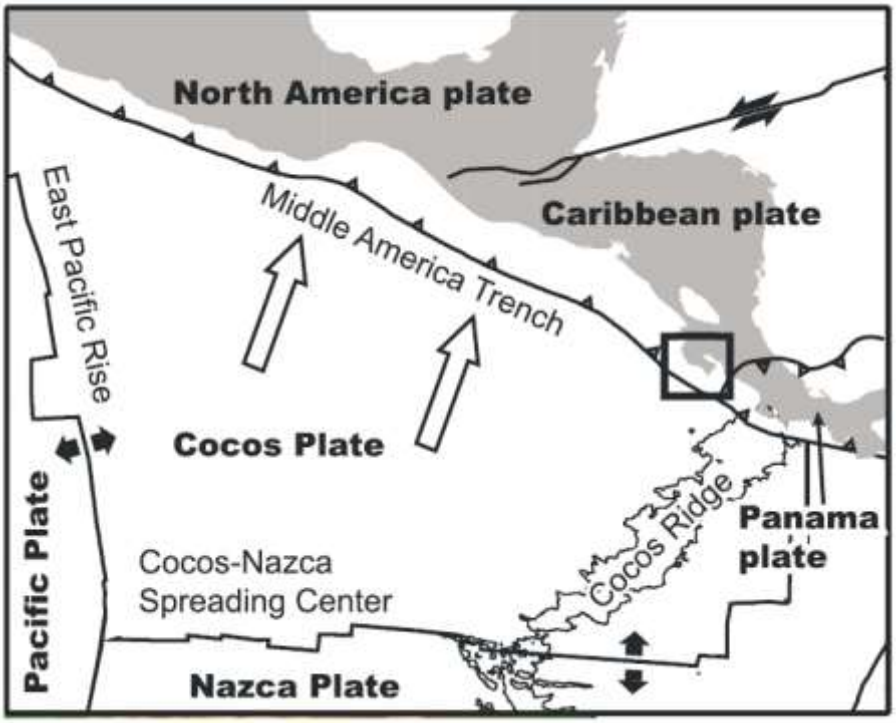

Figure 1. Map of the regional tectonic plate setting. The Cocos Plate subduct beneath the Caribbean Plate with the Middle America Trench created at the plate boundary. Notice the East Pacific Rise (EPR) spreading center to the west and the Cocos-Nazca Spreading Center (CNS) to the south, both contributing to characteristic subducting geology beneath Costa Rica.

beneath Nicoya. Land-based seismicity studies can be performed along this subduction megathrust that typically would require offshore seismometer deployment.

This research, which was performed as part of a Keck Geology Consortium project in Costa Rica, expands upon preliminary seismic studies on the Nicoya Peninsula following the recent M_w = 7.6 Nicoya Earthquake that occurred on 5 September, 2012. This project was broken up into three segments. The first segment, fieldwork on the Nicoya Peninsula, consisted of deploying a local seismic array as well as collecting data from already deployed stations on the peninsula. The second segment of this project consisted of identifying earthquake events found in the data, and the third segment of this project consisted of interpreting the seismicity that struck the Nicoya Peninsula approximately 9 months following a significant megathrust event. Relating this recent earthquake analysis along a recently ruptured subduction megathrust to previous comprehensive seismic studies in the area will contribute to the greater understanding of earthquake activity and aftershock seismicity, providing support for previous plate interface hypotheses in this study area.

Tectonic Setting

As part of the Central American convergent margin, the Middle America trench (MAT) runs from the Riviera fracture zone offshore Mexico to the Cocos ridge offshore Costa Rica, generating significant seismicity clearly defined along a Wadati-Benioff zone where the Cocos Plate subducts beneath the Caribbean Plate (Ranero et. al, 2008). In the early 1960s, a morphologically rough and smooth bathymetric boundary was identified (Fisher, 1961), and a multibeam bathymetric survey performed in the 1990s off the Nicoya coast, which showed smooth seafloor derived from the East Pacific Rise (Barckhausen et al., 2001, Schwartz and DeShon, 2007, Figure Bx). Just to the south of the EPR-derived crust is oceanic lithosphere derived from the Cocos-Nazca spreading center, CNS-1 and CNS-2, generated at the Galapagos hotspot.

There exist prominent bathymetric features on the rough CNS-2 segment, subducting beneath southern Costa Rica, including the Quepos Plateau, the aseismic Cocos Ridge, and the Fischer seamount group (Figure 2). It is hypothesized that this bathymetric roughness can generate seismicity (Protti et al., 1995), such as the 25 March, 1990 and 20 August, 1999 events with magnitudes $M_w = 7.0$ and $M_w = 6.9$, respectively, which have been attributed to the rupture of subducting seamount asperities off the coast of central Costa Rica. Bilek et al., (2003) linked these subducting seamounts to increased localized seismic coupling along the MAT, while Protti et al., (1995) noticed that the larger underthrusting earthquakes (M >7.5) have historically occurred to the north, where the seafloor bathymetry is smoother and where the plates are seismically coupled.

Because this convergent margin has the capability to create such large magnitude events, a joint seismic, geodetic and fluid flux study called the Costa Rica Seismogenic Zone Experiment (CRSEIZE) was performed from 1999-2001 with the deployment of both land-based and ocean-bottom seismometers onshore and offshore of the Nicoya Peninsula. This study relocated 650 earthquakes beneath the Nicoya Peninsula, with earthquakes located between 20 and 30 km in the northern part of the peninsula, while in the southern part of the peninsula, the updip limit of

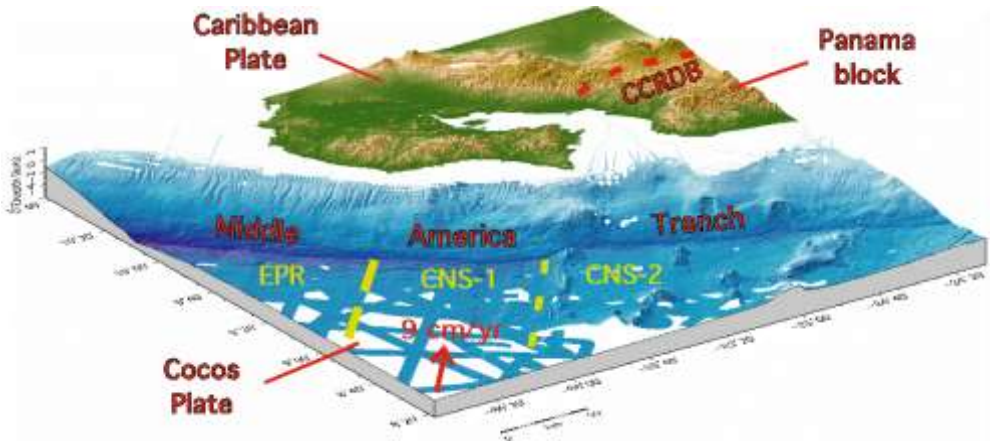

Figure 2. The Middle America Trench formed from the subducting ocean Cocos Plate beneath the continental Caribbean Plate, ~60 km off the coast of the Nicoya Peninsula, Costa Rica. Notice the smooth bathymetry of the East Pacific Rise crust (EPR) and the northern Cocos-Nazca Spreading Center crust (CNS-1), compared to the rough bathymetry of CNS-2.

earthquake hypocenters shallowed to approximately 10-13 km depth (Newman et al., 2002). It is believed that this variability in the updip and downdip limits of the seismogenic zone from the northern part to the southern part of the Nicoya Peninsula is due to a temperature difference of the EPR-derived crust and the CNS-derived crust. Fisher et al., (2001) state that heat flow changes across the EPR crust could contribute to a 70% cooler EPR crust compared to the CNS crust, causing these crusts to enter the trench at different thermal states.

While Newman et al., (2002) initially constrained the updip limit of the seismogenic zone at 10 km to the south and 20 km to the north along the Nicoya Peninsula, first noticing this change in focal depths from north to south, further studies performed by DeShon et al., (2006) more accurately constrained the seismogenic zone structure. By performing a simultaneous inversion of P- and S- wave arrival time data to solve for earthquake locations as well as to determine a three-dimensional velocity structure, DeShon et al., (2006) determined that plate interface microseismicity extends from 12 to 26 km beneath the southern Nicoya Peninsula, and from 17 to 28 km below the northern Nicoya Peninsula (Figure 3). Additionally, they noticed that microseismicity extended about 5 km closer to the Middle America Trench than what

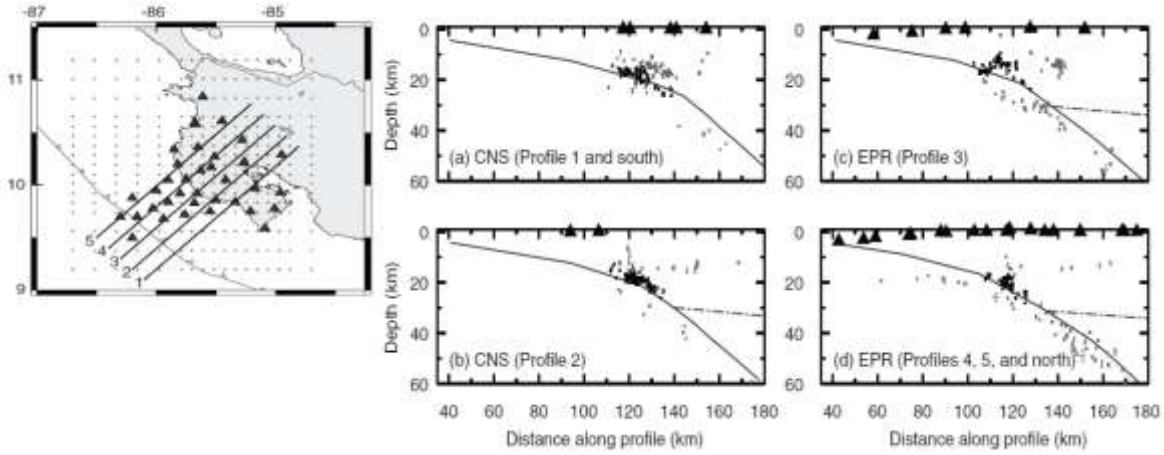

Figure 3. 5 transects across the Nicoya Peninsula with their respective cross sections, showing the seismicity and the variability of the seismogenic zone depth from north to south. Notice that in the south, the earthquakes are shallower than the earthquakes in the north, due to crustal differences of the subducting slab in the north versus the south.

Newman et al., (2002) had previously reported. Lastly, from tomographic studies along the Nicoya Peninsula, The EPR-derived crust is believed to subduct at a steeper angle than the CNS crust, because microseismicity within the EPR crust is located closer to the trench, from 75-88 km, which is approximately 12 km closer to the trench than the microseismicity identified within the CNS crust (DeShon et al., 2006, Figure 3). Thus, these CRSEIZE studies reveal that there exists significant variability in the seismogenic zone structure along the Nicoya Peninsula due to the significant EPR and CNS crustal differences.

Past Seismic Activity

Because the Nicoya Peninsula lies directly above the Costa Rica seismogenic zone, there has been a history of large underthrusting earthquakes with magnitudes greater than 7.5 that have ruptured along the Nicoya segment. With the Cocos oceanic plate subducting beneath the Caribbean plate at ~8 cm/yr, there exists a high seismic potential along the Nicoya Peninsula, with repeated M >7.0 earthquakes occurring in 1853, 1900, and 1950 with magnitudes >7.0, ~7.2, and M_w =7.8, respectively (Figure 4). Due to this ~50 year seismic cycle, a similar magnitude event was likely to occur, because other significant events in 1978 and 1990 did not rupture the seismic gap. Figure 5 is a schematic that represents the interseismic strain accumulation that builds up stress along the subducting plate interface. The plates are "locked", although some aseismic creep could also occur along the plate interface (Stein & Wysession, 2003). Since the 1950 event, interseismic strain has accumulated along the plate interface, and this accumulated strain as well as the coseismic deformation can be observed using both Global Positioning System (GPS) and geomorphic data (Protti et al., 2013).

Global Positioning System (GPS) can be used to develop detailed images of a locked plate interface and is helpful for understanding the mechanisms that control subduction zone seismicity (Protti et al., 2013). With a rapid convergence rate of ~9 cm/yr and the Nicoya Peninsula's proximity to the MAT, multiple geodetic studies have revealed that the converging oceanic Cocos

plate, which is assumed to be subducting at a constant rate, drags down the overriding Caribbean plate which creates large interseismic subsidence along the Nicoya coast and uplift farther inland (Lundgren et al., 1999, Feng et al., 2012). Prior to the 5 September, 2012 earthquake, Feng et al., (2012) performed GPS modeling to investigate if long-term coupling exists on the Nicoya subduction interface and where this coupling is the strongest. By using campaign and continuous GPS measurements, a coupling distribution model was created to determine where the most coupling occurs along the Nicoya subduction interface.

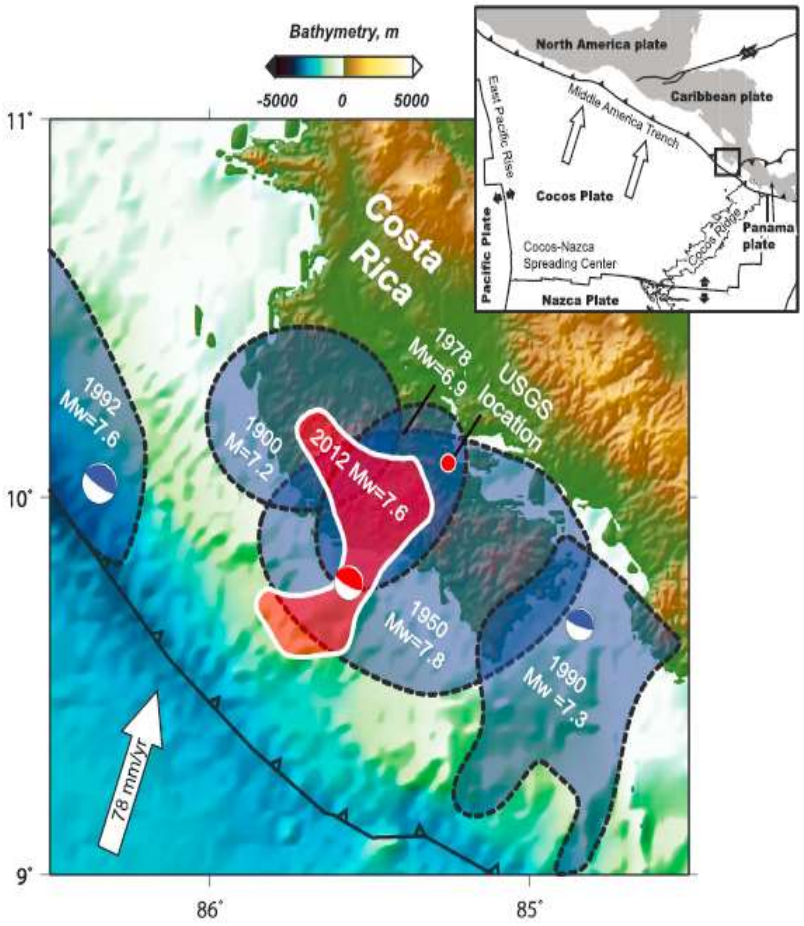

Figure 4. Estimated areas of rupture of all of the M>7.0 earthquakes since 1900 (Yue et al., 2013). The 1990, Mw =7.3 event ruptured the offshore area south of the Nicoya Peninsula. The 1992 event ruptured northwest of Nicoya along the subduction zone. The 1900 and 1950 events, which contains relatively uncertain but overlapping rupture areas, ruptured in the north and middle Nicoya. The coseismic rupture of the 2012 event is indicated in red, determined by Feng et al.,(2012).

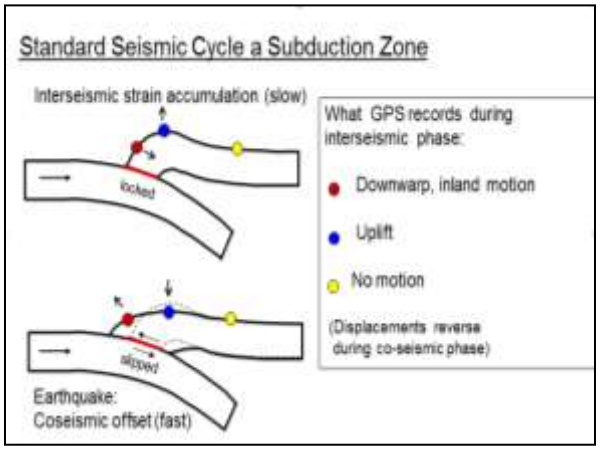

Figure 5. Schematic created by Dixon (2007), which shows the interseismic strain accumulation between large subducting earthquakes, and the coseismic offset that occurs when the elastic strain releases. The overlying and underlying plates are locked when no slip is occurring along the plate interface.

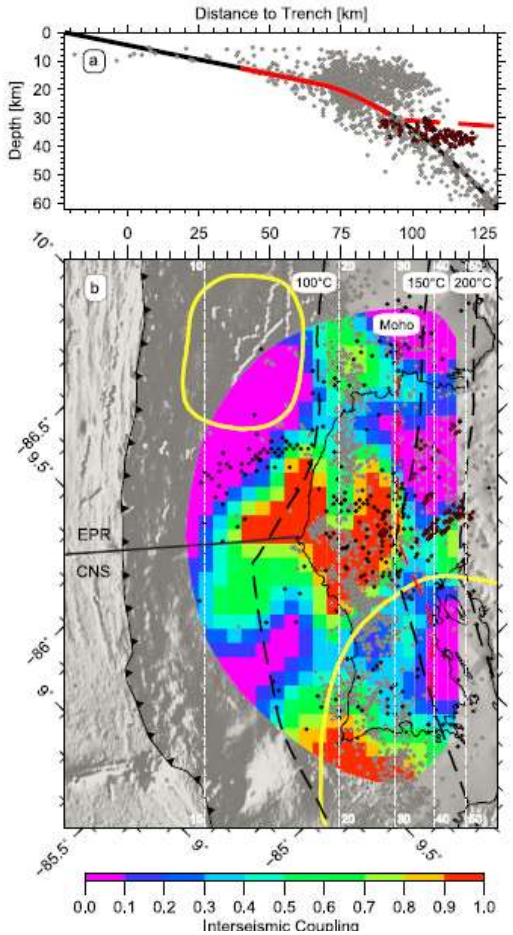

Figure 6. The preferred coupling model and a cross section of the subducting plate interface beneath Nicoya from Feng et al., (2012). In (a) the red line indicates the locked plate interface before the 5 September, 2012 earthquake. In (b) the red areas indicate the areas along the interface that are fully coupled, and the black contours indicate the various isotherm boundaries. The black dots represents tremors, an earthquake lasting a longer period of time than aftershock seismicity.

Figure 6 shows the preferred coupling model as well as interplate microearthquakes beneath the Nicoya Peninsula. The downdip extent of the fully coupled patch beneath Nicoya was located at 28-29 km depth (Figure 6a), and two fully coupled patches exist at ~15 km depth offshore and the other located at ~24 km depth more inland (Feng et al., 2012, Figure 6b). Thus, a potential M_w= 7.8 earthquake similar to the 1950 earthquake was expected to be generated from the rupture of those two fully coupled lock patches. Additionally, coastal topography can indicate whether deformation is occurring due to coupling along the plate interface. Indicators such as marine terraces, changing tides and the effects on the ecology, among others can be used to track deformation changes over time, specifically on the Nicoya Peninsula where the coast is extremely susceptible to these changes (Marshall & Anderson, 1995); however, the geomorphological aspects of the seismic cycle are beyond the scope of this paper.

As previously stated, the motivation for this seismology study on the Nicoya Peninsula stemmed from the M_w= 7.6 earthquake on 5 September, 2012 at 14:42:07 UTC, which partially ruptured the subducting plate interface between the Cocos and Caribbean plates, beneath the

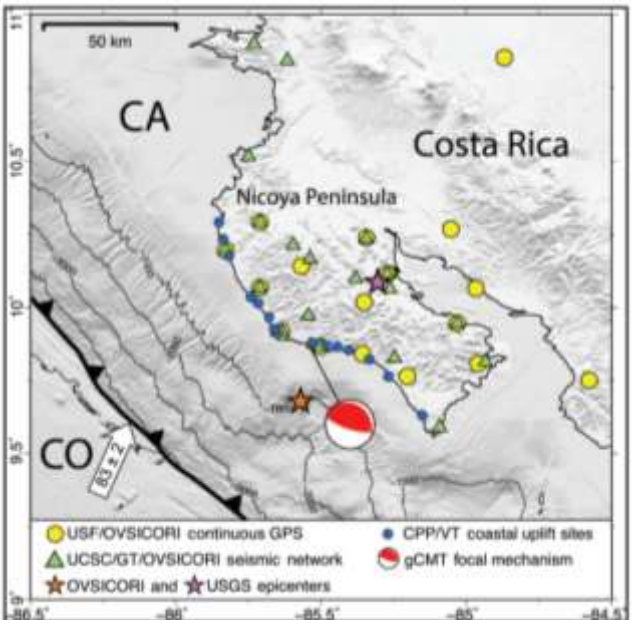

Figure 7. USGS and OVSICORI (Universidad Nacional), locations for Nicoya earthquake, and the global moment tensor solution (USGS), exhibiting a NE shallow-thrust mechanism. GPS and seismic sites indicate by the circles and triangles, respectively.

Nicoya Peninsula, Costa Rica (Yue et al., 2013). Initially, the United States Geological Survey (USGS) located this event in central Costa Rica at 10.085ºN, 85.315ºW, with a hypocenter depth of 35 km. However, Yue et al., (2013) utilized GPS, ground-motion data, as well as P-wave observations to relocate the event offshore, at 9.76ºN, 85.56ºW, at a depth of 13.1 km BSL and ~10 km away from the coastline (Figure 7).

The USGS and OVSICORI hypocenters were located in different locations, because typically the USGS does not use regional or local seismic networks when locating global earthquakes. However, since the Nicoya Peninsula already contained an extensive network of both GPS and seismic stations operated by OVSICORI (Universidad Nacional), that hypocenter was used as the more accurate location. Using these multiple campaign and continuous GPS sites, the amount of coseismic rupture, or the amount of slip that occurred along the fault during the

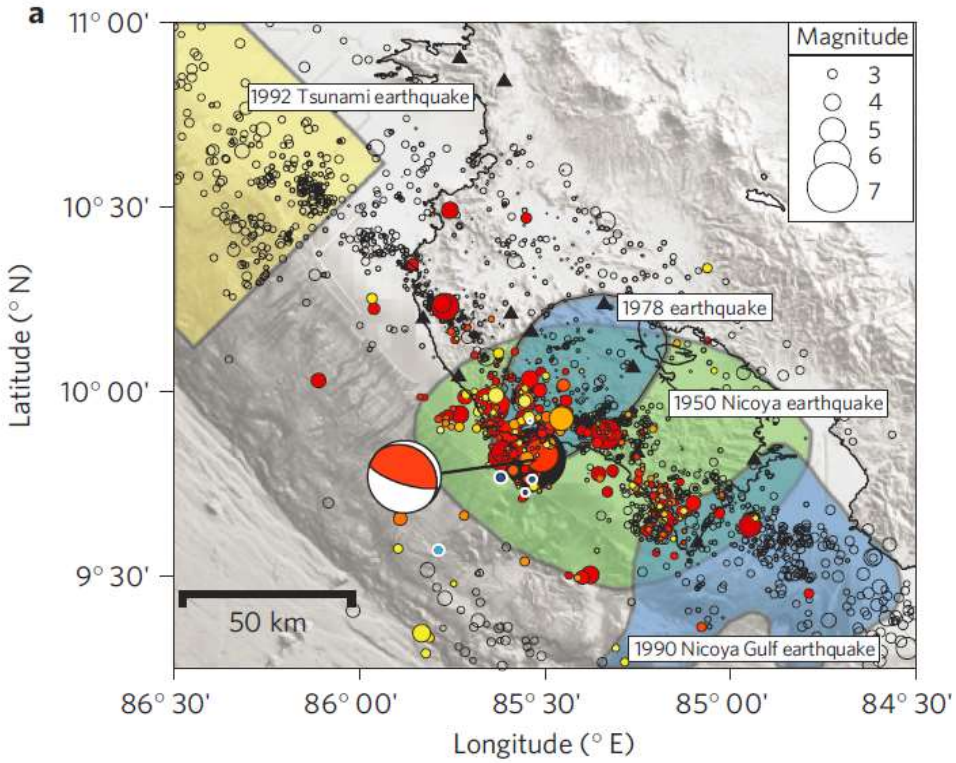

Figure 8. The location of the 5 September, 2012 earthquake and surrounding aftershock seismicity colored by the timing of the events (red=early aftershock, yellow=later aftershocks). The focal mechanism (beach ball) was a complete thrust event with a rake of 102º. Black circles represent past microseismicity along the Nicoya Seismic Gap.

earthquake, was 4.3 meters of thrust and 1.1m of right-lateral motion, with an average rupture velocity of 3.0 km/s (Yue et al., 2013). From the hypocenter, the earthquake propagated downdip, which means the rupture was primarily beneath the Nicoya Peninsula (Protti et al., 2013)(Figure 8).

The Nicoya earthquake partially ruptured the previously identified locked patch of the subduction plate interface, the area of the plate interface that is creeping at less than 50% of the ~9cm/yr convergence rate (Protti et al., 2014, Figure 9a). However, further GPS analysis of the area of rupture following the 2012 earthquake revealed that the fully coupled region updip and offshore of the Nicoya Peninsula did not rupture (Figure 9b). The offshore region has the potential to rupture in the future since that area did not release the

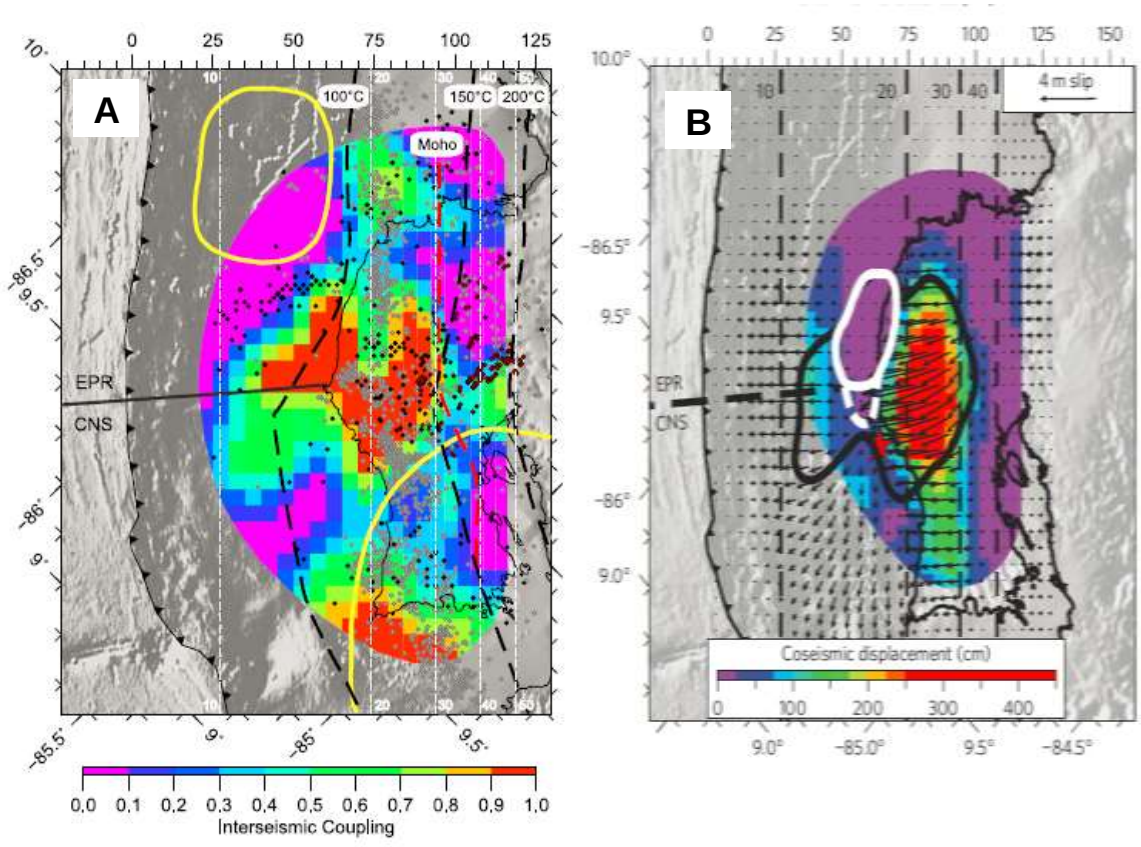

Figure 9. Interseismic and coseismic coupling models from before the earthquake (Feng et. al (2012)) (a) and following the earthquake (Protti et al., 2014) (b). **(a)** Red area indicates the area of the plate interface that is fully locked. **(b)** The circle white region represents the area following the earthquake that did not rupture, while the onshore area of the previously locked patch did rupture.

accumulated seismic strain from the last megathrust event in 1950 (Yue et al., 2013). Due to the comprehensive seismic and GPS monitoring that has taken place in the past decade on the Nicoya Peninsula and the anticipation of such a large event to occur, heightened awareness of this earthquake risk resulted in no confirmed human deaths (Protti et al., 2014).

METHODS

Seismometer Equipment Used

The Keck Geophysics team set up 5 seismic stations directly above the area of rupture of the 5 September, 2012, M_w= 7.6 earthquake. Each station consists of one Nanometrics Taurus Digital Seismograph (Figure 10), a Taurus digitizer, a battery pack, a GPS receiver, and a solar panel. The seismic data is logged onto 2-4 Gb hard disks, which are stored inside the Taurus digitizer and its protective casing. The solar panel, which attaches to the top of the casing that holds the digitizer, powers the seismometer while exposed to sunlight, and an external battery powers the seismometer, which is charged by the solar panel, when there is no sunlight. These

Figure 10. Trillium Compact Seismograph with labeled parts. The bull's eye on top is used for levelling seismograph in the ground, using the feet with locking mechanisms. Seismograph must be aligned north. The cable port connects to Taurus Digitizer located above ground.

seismographs were used as opposed to other broadband seismometers, because they are suitable for long deployments, data retrieval is not complicated, and the transport of the equipment is condensed into a single casing for easy maneuverability in the field. The data output onto the hard discs was in miniSEED format, which was later converted into SEISAN format for processing.

Building A Seismic Station

When deploying a seismic station, the first step is to dig a hole ~0.5-1 m deep to completely bury the seismograph (Figure 11). Once the seismograph is placed into the hole, it must be leveled, which is performed by adjusting three feet on the bottom of the Taurus

Figure 11. Initial steps involved in setting up the seismograph in the ground. **(a)** Digging a 0.5-1m hole to bury the seismograph. (**b)** Covering the seismograph with plastic to protect against water damage. **(c)** PVC casing placed around seismograph to secure it in place. **(d)** Aligning seismograph towards north.

seismograph until the bubble on top of the seismograph is located directly inside the bull's eye (Figure 10). A PVC casing is placed around the seismograph as well as a plastic bag to both secure the seismograph in place and to inhibit excess water coming into contact with the seismograph (Figure 11b & 11c). Once the seismograph is aligned towards north, the cable connecting the seismograph to the Taurus digitizer is connected (Figure 11d).

Once the seismometer is buried, the cable connected to the seismograph must connect to the Taurus Digitizer above ground (Figure 12a). Inside the digitizer, two either 2 Gb or 4 Gb hard disks are inserted, which record all of the seismic data. The Taurus Digitizer connects to the battery source, which receives its power from a solar panel attached to the top of the blue protective case. Once all pieces are connected, a barbed wire fence is built around the seismic station. To verify the seismograph is recording correctly, a jump test is performed, in which one

Figure 12. Additional seismic station setup. **(a)** Digitizer hook-up to seismograph and battery. **(b)** Fence built around station to protect against outside disturbances. **(c)** GPS taped to fence post to record accurate time. **(d)** Final setup in blue protective casing, with solar panel attached on top.

jumps adjacent to the buried seismometer to verify the seismograph is recording seismic signals that can be viewed on the digitizer. Next, a GPS receiver is installed on one of the fence posts, which is used to record accurate timing while the digitizer is recording data (Figure 12c). Lastly, everything should be in working order, and the blue protective casing is ready to be closed until data retrieval.

Station Deployment and Locations

The first seismic station was deployed at the Lagarta Lodge (LALO), the Keck base lodge ~3.5 km from central Nosara, a coastal Nicoya Peninsula town that significantly felt the mainshock in September (Figure 13a). At 9º 57.90'N, 85º40.61'W and 56 m above sea level, LALO was located ~0.5 km from the coastline (Figure 14), buried adjacent to the bar area of the Lodge. LALO was deployed on 26 June, 2013, at 0800 UTC, the earliest station deployment in the KECK network.

The second seismic station, SAMA was deployed ~ 2 km from Playa Sámara and ~20 km south of LALO along the western Nicoya coast (Figure 13c). The location of this station, at 9º53.350'N, 85º32.920'W and 52 m above sea level was chosen because there already existed a GPS monument created as a campaign GPS site during the CRSEIZE experiment (Figure 14). SAMA was deployed on 2 July, 2013 at 1100 UTC, and because SAMA was located on private land, a fence was built around the seismic station to protect against animal interference (Figure Dyc).

The third seismic station, MIRM, was deployed ~17 km inland from SAMA and ~14 km inland from LALO (Figure b) at 10º02.53'N, 85º34.27'W at 439 m above sea level (Figure 14). MIRM represents the inland apex of the triangular area formed by the other two stations, LALO and SAMA. The third seismic station deployed on 2 July, 2013, was GUIO, which represents the station < 0.5 km from Playa Guiones and ~2 km from the 'elbow' of the Nicoya Peninsula (FIgure 13d). Located at 09º55.38'N, 85º39.51'W and 39 m above sea level, GUIO was also located adjacent to a previously used GPS monument, on a 'gumdrop' hill adjacent to the main

road connecting Guiones with other coastal towns. The final seismic station deployed, GRAS, was deployed on a private farm directly in the center of the triangular area formed by LALO,

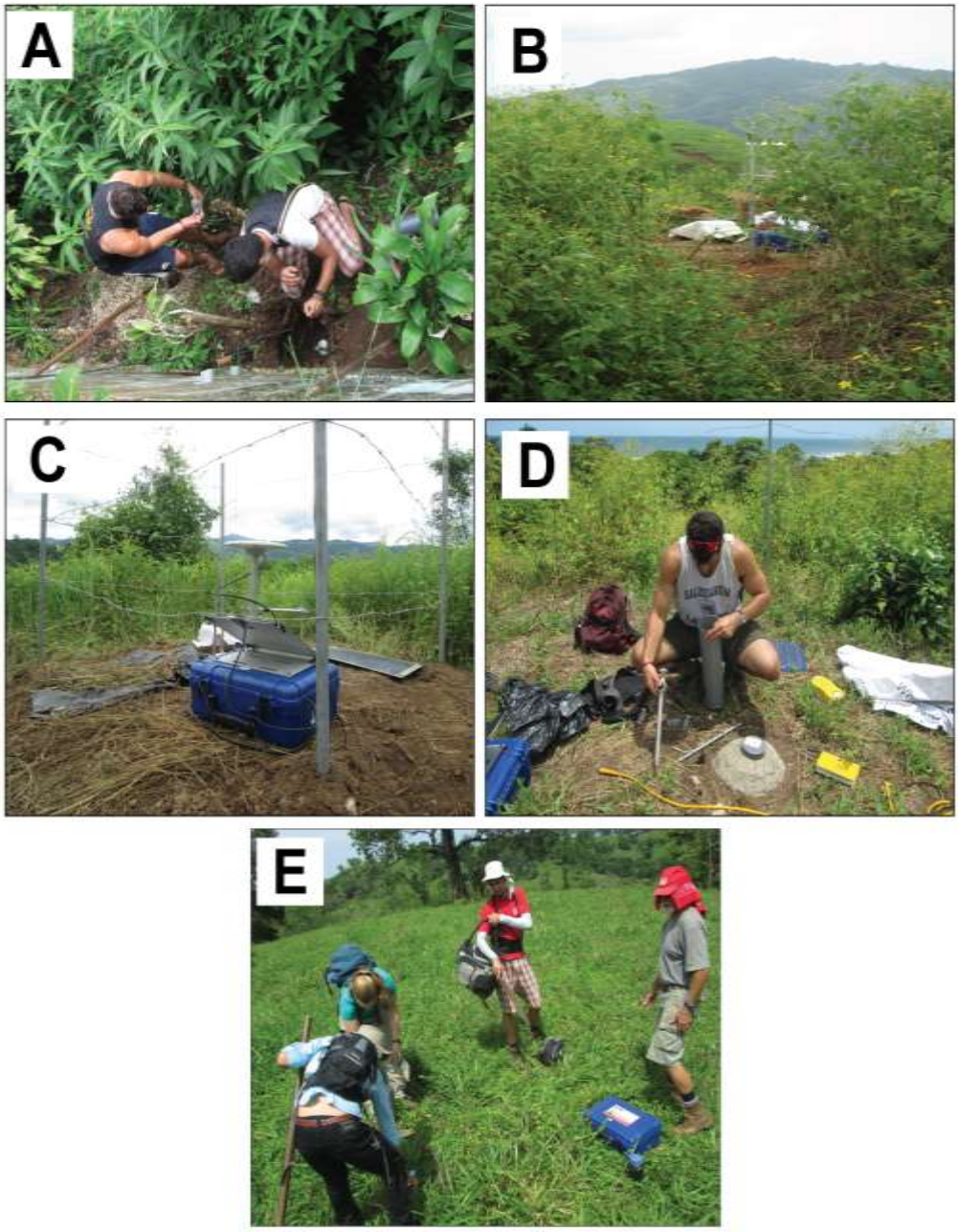

Figure 13. Photos of each KECK Network station on the Nicoya Peninsula, Costa Rica. **(a)** LALO, the Lagarta Lodge Station in Nosara. **(b)** MIRM, near the town of Miramar. **(c)** SAMA, near Playa Samara, on private grazing land. **(d)** GUIO, on a gumdrop hill adjacent to Playa Guiones, on grazing land for cattle **(e)** GRAS, near the center of the four other stations in farmland on private property, named after Greg-Richard-Anthony-Shannon, the names of the four students.

SAMA, and MIRM (Figure 13e). GRAS was deployed on 9 July, 2013 at 9º56.59'N, 85º34.58'W, at 236 m above sea level (Figure 14).

Figure 14. Location Map for the 5 KECK network stations on the Nicoya Peninsula, Costa Rica with an inset of the area of coseismic coupling following the 5 September, 2012 earthquake. Notice the KECK station is directly above the area of coseismic rupture, identified by the red area in the inset.

Since monitoring did not begin until 26 June, 2013, seismic data taken from stations affiliated with the Nicoya Network were also used to supplement the KECK Network data. These continuous seismic stations include HATI, PNE2, NARJ, ARDO, INDI, and SAJU (Figure 15), which are maintained by OVSICORI, associated with UNA (Universidad Nacional, Costa Rica). These stations are also permanently installed for longer deployments, in which a deeper hole is dug to place the seismometer in order to reduce the amount of background noise that can affect the seismic signal.

Acquiring the Seismic Data

Because the seismic signals acquired by the KECK stations could not be accessed remotely, on 17 July, 2013, the data from each station were removed and the campaign stations

were taken down. Deconstructing the seismic site required that the digitizer recording the data be shut down. Next the seismometer must be dug up from where it was buried and assuring that nothing was tampered with during the time of data collection. Other than slight corrosion on the outside of the wire connecting the digitizer to the seismograph at the SAMA station, there existed no problems with the stations during the data collection period. Additionally, the hard discs that recorded the data in the digitizers were collected and downloaded onto respective computers to be prepared for analysis.

Figure 15. Nicoya Network Stations. Stations used for this study are HARI, JUDI, INDI, GRZA, ARDO, and SAJU. Other Nicoya Network Stations were either offline or recorded noisy seismic signals that couldn't be used for analysis.

Data Conversion into SEISAN format

The seismic analysis software used to process all of the collected data from the KECK and Nicoya Network sites was Seisan (Haskov and Ottemöller, 1999), a seismic analysis system with a set of programs that analyzes earthquakes within a database. This program was used, because Seisan is a free seismic software package that still consists of programs that are useful for earthquake characterization. Typically, data from seismic stations is saved in the Standard for the Exchange of Earthquake Data (miniSEED), a format most commonly used when storage of large amounts of earthquake files is needed; however, SEED volumes are typically not designed for

data processing and are typically converted into other formats for data processing, such as the SEISAN format (http://www.iris.edu/dms/nodes/dmc/data/formats/#miniseed).

The miniSEED files taken from the Taurus digitizers are separated by one-hour time intervals, with each station using three components, up-down (Z), north-south (N), and east-west (W) to determine the simultaneous earth movement in all directions. For each hour from the start of data acquisition to the end of data acquisition, every N,Z, and W file for each station that was online for that specific hour must be converted into Seisan format, a file format that allows for seismic analysis in Seisan. Once all of the files were converted, all Seisan files for each hour from each station were merged together, so that earthquake picking on each station can be performed (Figure 16).

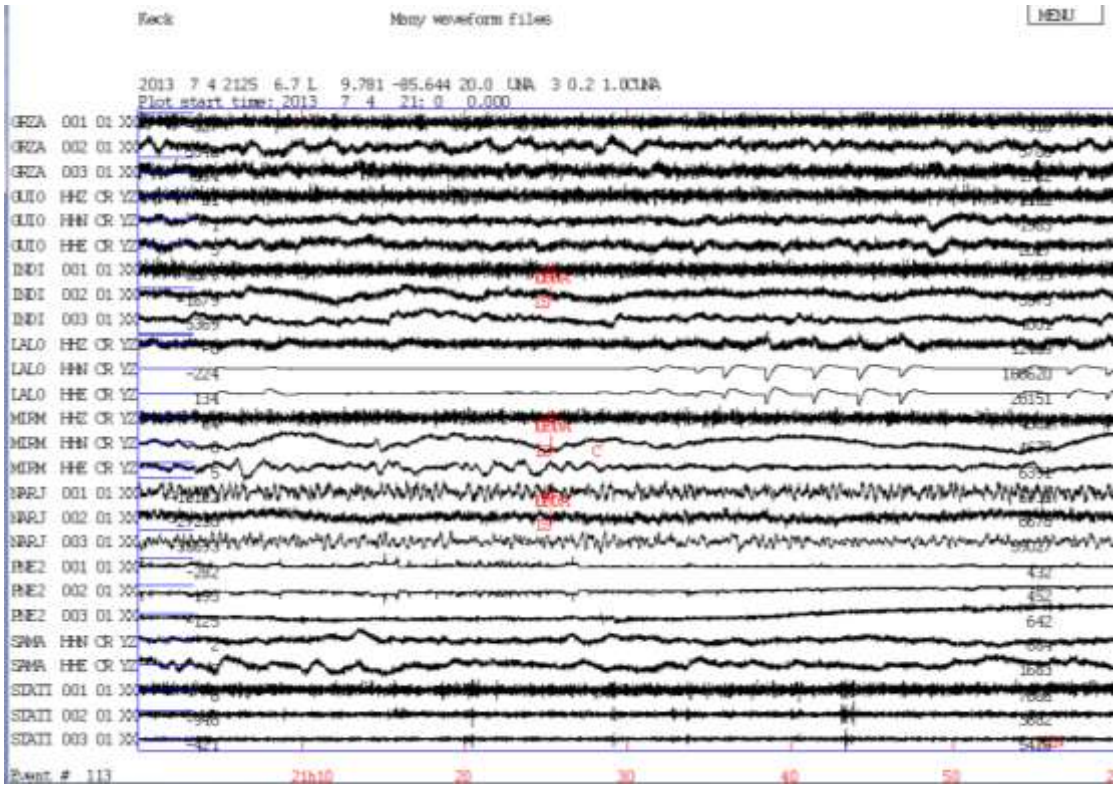

Figure 16. Interface of an hour-long time interval of seismic data from multiple stations on 4 July, 2013 at 2100-2200 UTC. Notice each station contains three components, corresponding to the vertical, north-south, and east-west directions. Each four letter abbreviation to the left (i.e. GRZA, GUIO) are the different station names.

Picking of Earthquake Events

After the station files were converted and merged for each hour, the next step in the process of earthquake processing is identifying events in the data. In order to identify earthquake events, the earthquake signal-to-noise ratio must be reduced so that identification of earthquake waves can be performed. Thus, filters must be used to attenuate frequencies that do not pertain to the earthquake frequency range. Because the Taurus seismograph are broadband seismometers, meaning that they record seismic signals over a wide frequency range (0.01 – 50 Hz), earthquake signals can be filtered out of the wide range of frequencies that make up the seismic signals, since earthquakes typically have frequencies of 0.5-20 Hz. There exist high-pass, low-pass, and band-pass filters that cut out low frequencies, high frequencies, and both high and low frequencies, respectively.

The first step in identifying earthquake events in each hour-long file required applying a band-pass filter to attenuate very low-frequencies and very high-frequencies that could be attributed to noise from car traffic, ocean waves, animal interference, and other sources for non-earthquake noise (Figure 17b). Once that filter was applied, the file was scanned for identical peaks, or similar waveforms evident on each station, because if there exists a similar peak across each station, then it can be assumed that the source of that peak is not local to just one station, but rather something such as an earthquake must have contributed a seismic wave to all stations. In Figure 17, only the Z-component is shown, which would clearly show a P-wave arrival since P-waves travel compressively up and down. As shown in Figure 17b, an apparent waveform is across all stations is evident early in the data. Then Seisan has the capability to zoom in and decrease the time range, enhancing that specific waveform (Figure 17c). Thus it is evident that a waveform exists, and Figure 17d confirms this, in which another 5-10 Hz bandpass filter was applied to reduce the noise even further. The characteristic earthquake waveform is clearly seen

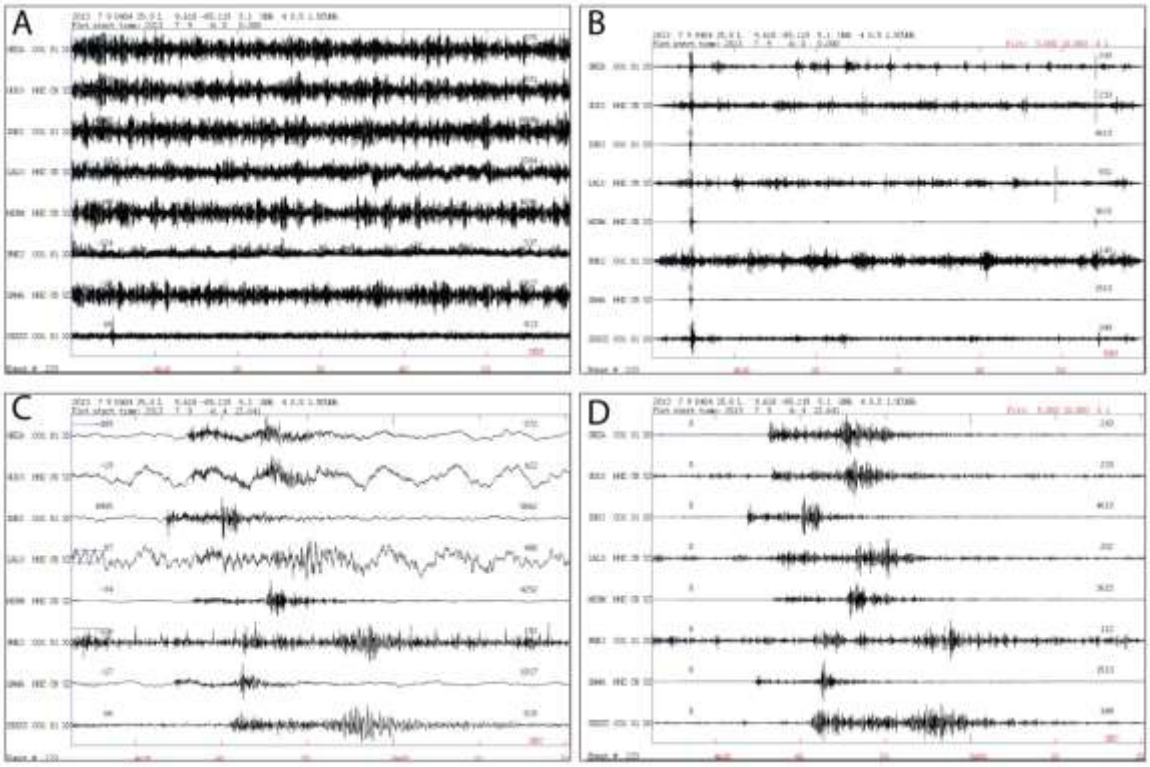

Figure 17. Example of process performed to identify earthquake events in the database. **(a)** Unfiltered, hour-long data for 07/04/2013. **(b)** A 5-10 Hz Band-Pass Filter Applied over same data over same hour. Notice the identical waveform early in the hour. **(c)** Zoomed-in to peaks those identical peaks with no filter applied. Notice the waveform resembles an earthquake. **(d)** Applied another 5-10 Hz filter to reduce signal-to-noise ratio and show that an earthquake clearly exists.

across all stations, and thus this event was logged as an earthquake.

RESULTS

Vp/Vs and Velocity Structure

All earthquake events were first located using a reference travel time curve, IASP91 (Kennett & Engdahl, 1991), a model constructed from global, travel-time characteristics of the main seismic phases, or the change of seismic velocities within the earth. Although this model is not an accurate local representation of the earth structure beneath the Nicoya Peninsula, locating earthquakes using this global model is useful for preliminary analysis, ensuring that the earthquakes are not plotting in locations far from where they are expected to be located. Figure 18 shows preliminary earthquake locations using the IASP91 velocity model. From June 23 to

July 18, a total of 261 events were located using this model (Insert Table of IASP91 Data in Appendix). The average RMS value for these 261 events is 0.3 ± 0.7.

To reduce the RMS values of these events, a Nicoya-specific velocity model is used in replacement of the IASP91 model, to produce more accurate earthquake locations on the Nicoya

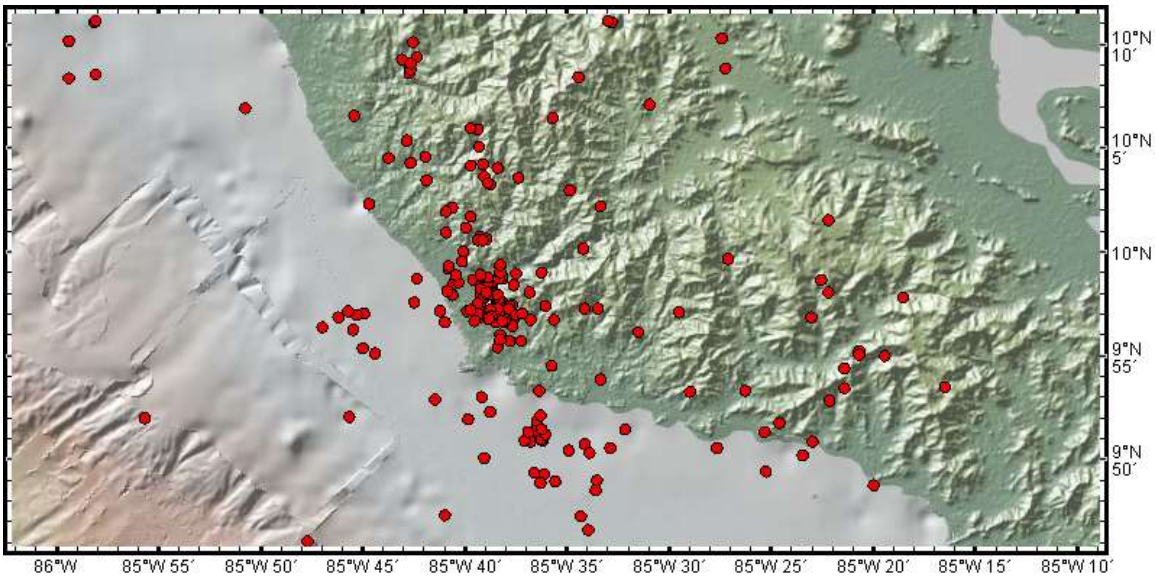

Figure 18. Initial earthquake locations using the IASP91 velocity model, a model created from average global travel times not specific to the Nicoya Peninsula. 261 earthquakes, both local and regional events, were identified and initially located using this model.

Peninsula. DeShon et al. (2006) created a 1D P-wave velocity model with velocities specific to the earth structure beneath the Nicoya Peninsula, which was calculated using CRSEIZE Nicoya arrival time data (Insert velocity model Table in Appendix). A total of 254 events were relocated using the new velocity model. This number is 7 less than the number of events located in the IASP91 model, because these 7 events were regional events not located beneath the Nicoya Peninsula which recorded abnormally high time residuals (RMS) than the other events located locally. The average RMS value of the 254 events using the DeShon velocity model was 0.27 ± 0.62, which is a lower average time residual than with the IASP91 model. In other words, the

travel times of these located events were closer to the expected travel times than when the IASP91 velocity model was used.

Once the DeShon model was used to relocate the events, taking into account the high and low velocities apparent on the Nicoya Peninsula, the final procedure was performed to check if the calculated travel times could be correlated any better with the expected travel times of each event. The Vp/Vs ratio versus the average RMS value of the events was compared. When performing previous earthquake analysis on the Nicoya Peninsula, Protti et al., (1995) used a Vp/Vs ratio of 1.78, a value also consistent with previous seismic studies. To verify that this Vp/Vs value would be suitable for this earthquake analysis project, a range of Vp/Vs values, from 1.75 to 1.80 with a 0.01 increment, were used to see if another Vp/Vs ratio other than 1.78 would reduce the average RMS values of the events. Figure 19 shows this comparison, and it is apparent that the RMS and standard deviation for 1.78 is just slightly lower than those with the Vp/Vs ratio of 1.77. Vp/Vs ratios below 1.77, at 1.76, and 1.75, show increased RMS and standard deviation values. Thus, the Vp/Vs value used for this study kept at 1.78, since no other Vp/Vs value significantly reduced the average RMS value of these events (Figure 19, Table X).

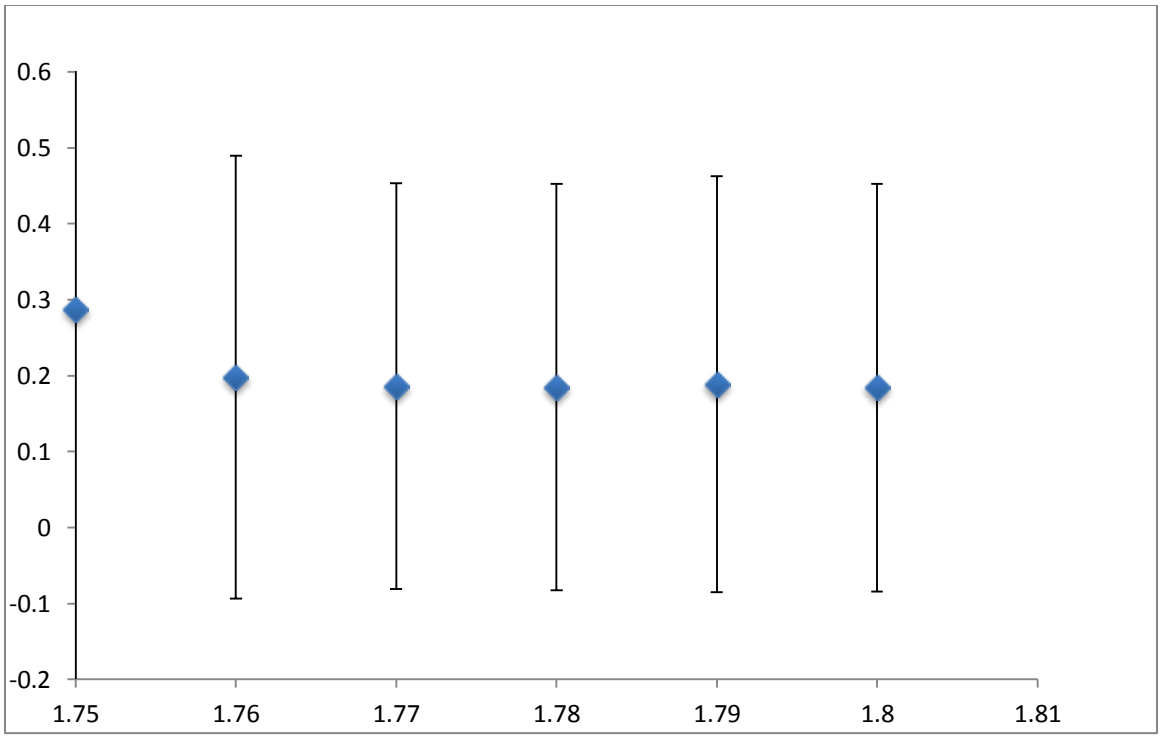

Figure 19. Vp/Vs value along the x-axis, and RMS value along the y-axis. A Vp/Vs value of 1.78 corresponds to the lowest RMS value, thus 1.78 is the Vp/Vs value this is used for the earthquake locations.

Comparison of IASP to DeShon

Figure 20 shows the different earthquake locations on a regional scale using the two different velocity models around the Keck network stations, plotted as the yellow triangles. Notice the earthquake epicenters around the Keck network using the Nicoya-specific velocity model plot in separate locations than when using the IASP91 velocity model (Figure 20). A specific example of earthquake location differences using these two different velocity models is shown in Figure 21. On 23 June, 2013 at 20:00:35 UTC, an earthquake with magnitude Mw above 5.0 was recorded on the Nicoya Peninsula, located 5 km northwest of Playa Garza, Guanacaste at 9°58'26.4"N, 85°39'35.9"W, whereas the same earthquake was located within 5 km of the LALO Keck Station and < 10 km from the GUIO Keck station using the Nicoya-specific velocity model

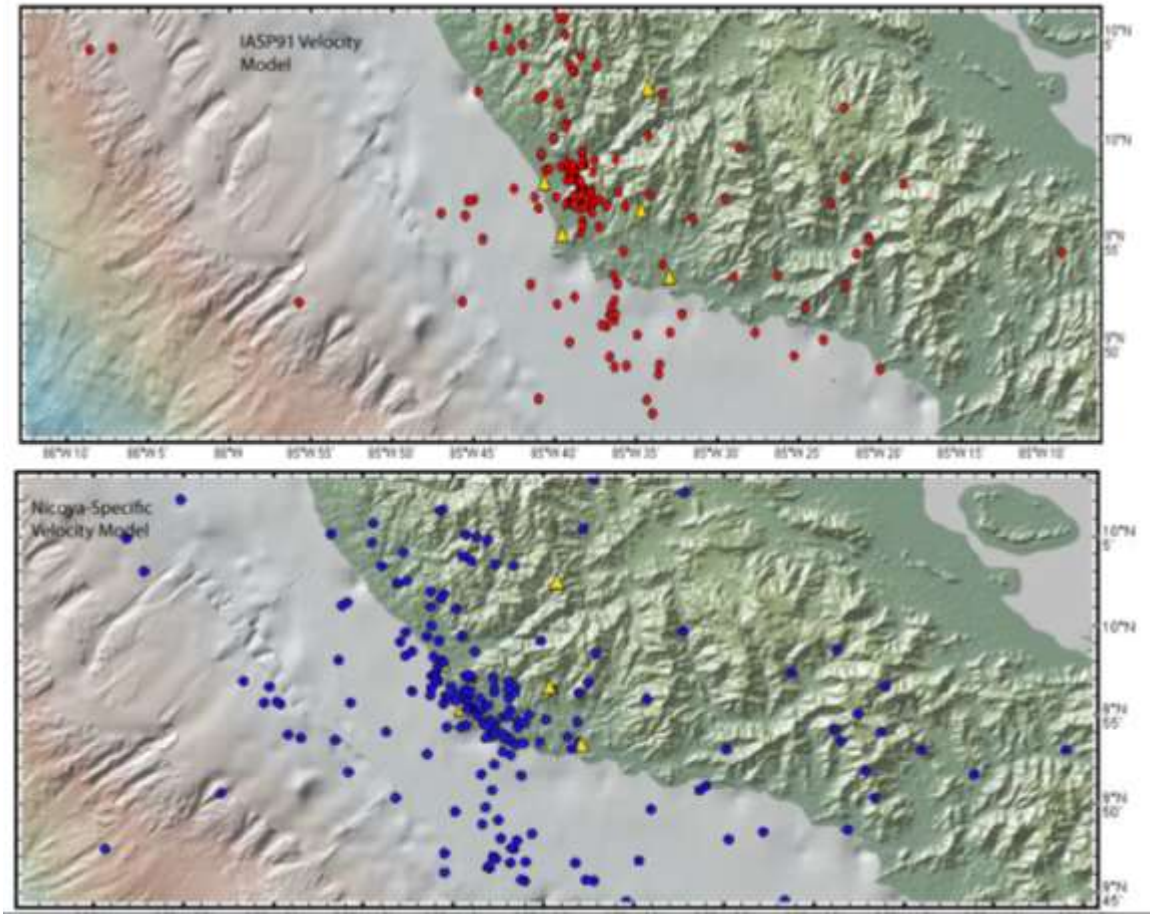

Figure 20. Earthquake locations using the IASP-91 velocity model and the Nicoya-specific velocity model. Notice the difference in epicentral locations due to the different velocities. The Nicoya-specific model is used in the rest of the aftershock analyses.

(Figure 21). Not only do the epicentral locations differ, but the hypocentral depths also vary, with 21.5 km and 15.4 km calculated using the IASP91 and the DeShon model, respectively. This comparison illustrates the importance of determining the velocity structure beneath the study area and then implementing that velocity structure when performing analyses that depend on an accurate representation of crustal structure.

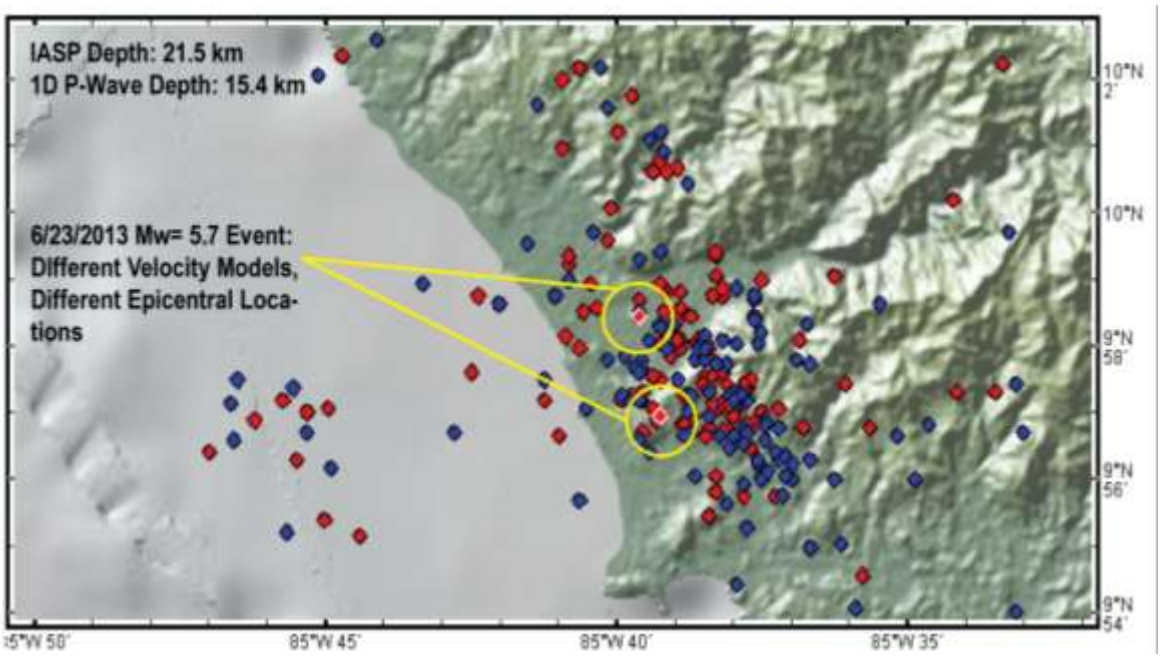

Figure 21. The June 23rd, magnitude 5.7 earthquake event located using the two different velocity models. The IASP-91 model, in red, locates the earthquake to the south, while the Nicoya-specific velocity model, in blue, locates the event to the north. The Nicoya-specific velocity model will be the model used for the additional earthquake analysis.

June 23rd Event

As previously stated, 254 events were identified in the seismic data, collected from June 23 to July 18. 39 earthquakes were identified on June 23 as a result of the Mw= 5.7 earthquake that occurred directly within the study area. Of those 39 earthquakes, one earthquake occurred approximately 25 minutes before the mainshock with a magnitude of 1.6, indicated by the yellow circle overlain by the blue circles (Figure 22). This foreshock is located approximately 5 km southeast of the mainshock, with a calculated depth of 20.9 km. The three other earthquakes are located outside the network and are assumed to be unassociated with the mainshock. The June 23rd aftershocks within the area of the Keck network have depths ranging from 15.3 km to 26.3 km. The average depth of these aftershocks is 18.5 km. The magnitude of these aftershocks ranged from 0.6 to 1.3, with an average magnitude of ~0.9.

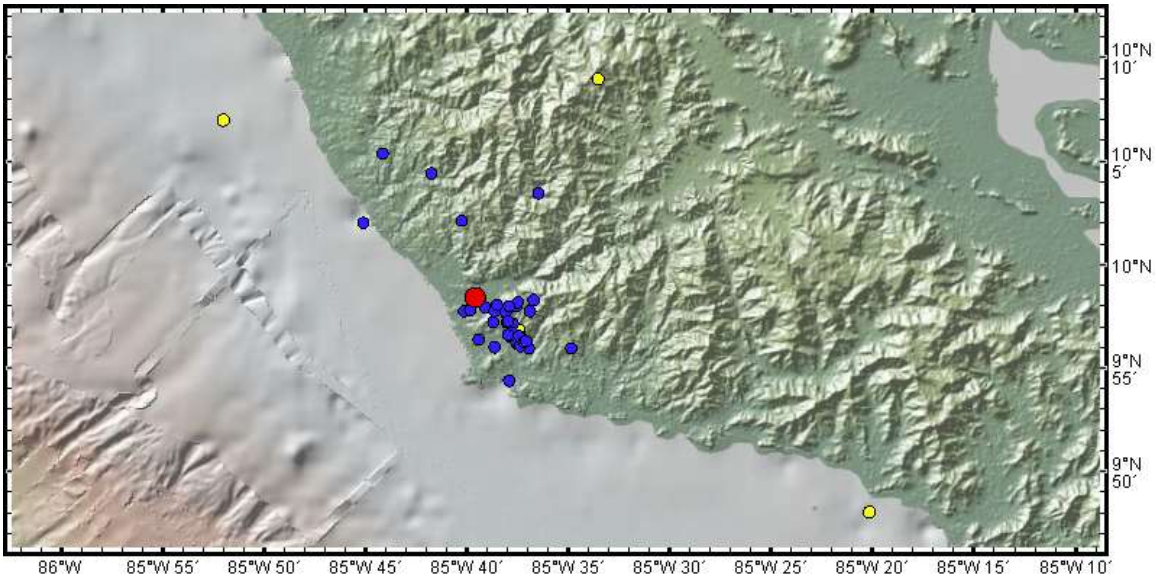

Figure 22. The June 23rd aftershock (in red) and the earthquakes identified both before the event (in yellow), and all earthquakes identified on June 23 following the Mw= 5.7 event (in blue).

Depths and Magnitudes

After June 23rd, the number of earthquakes dropped to 25 on June 24th, stabilizing to 1-5 events for the remainder of June (Figure 23). For the remainder of station deployment, through July 18, 214 events were recorded. Of the 254 events recorded in the database, 191 earthquakes were calculated at depths between 16 and 24 km (Figure 23). 64 events had focal depths between and 28 km, and 26 events had depths greater than 28 km. Specifically within the 5-station Keck network, 155 earthquakes were recorded, with 106 of these earthquakes having focal depths of ~20 km (Figure 24). In close vicinity to the Keck network, 30 earthquakes recorded magnitudes greater than 1 (Figure 24). The largest magnitude earthquake within the network following the June 23 event occurred on July 5, 1317 UTC at 9°57'43.1994"N and 85°36'39.6"W with a magnitude of 1.4. The events within the Keck network also recorded magnitudes of ~0.3 to 1.2. Lastly, there is a cluster of events located off the coast of the Nicoya Peninsula to the southeast of the network, which had focal depths that were slightly shallower than the focal depths of the earthquakes further inland, at ~17-18 km (Figure 24).

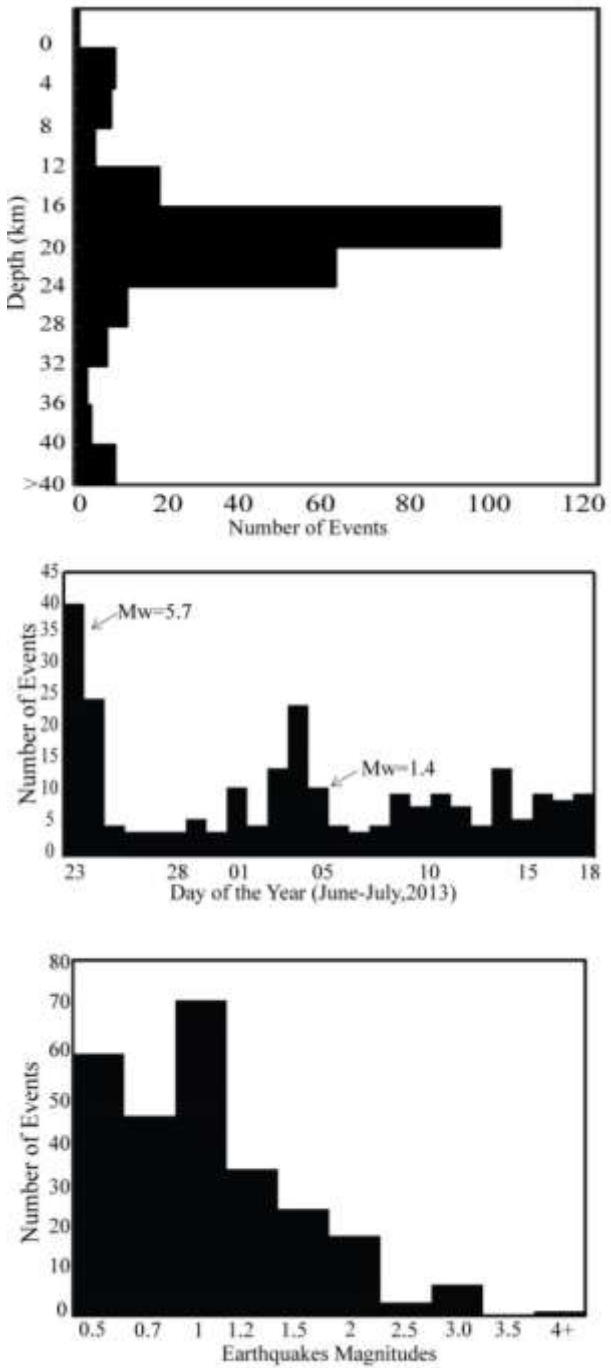

Figure 23. Histograms created from the located earthquakes in the database. Of the 261 events, 191 of those events were located between 16 and 24 km. The rest of the earthquakes either were shallower or deeper interplate earthquakes in either the Caribbean or Cocos Plate. The spike in events on June 23-24 is associated with the aftershock seismicity from the M_w= 5.7 event. Notice that most earthquakes were less than or equal to magnitude 1.0.

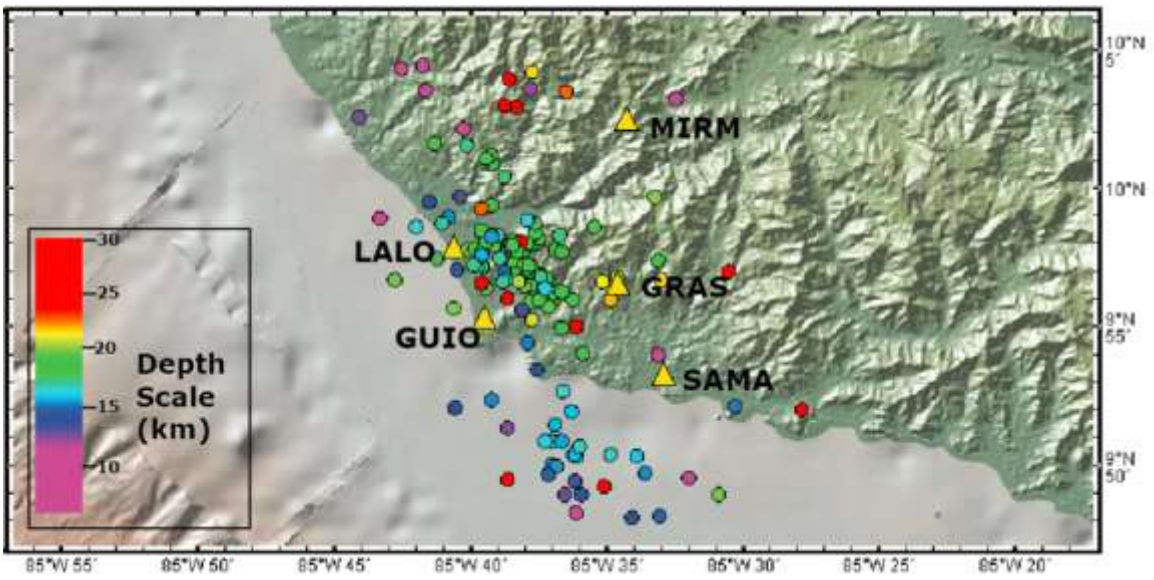

Figure 24. Depth of earthquake locations locally around the Keck Network stations, identified by the yellow triangles. Earthquakes to the north have focal depths at ~20 km, while earthquakes to the south have focal depths at ~15 km.

Waveform Correlation

Following earthquake relocation, waveforms within the Keck network were analyzed to identify instances of multiple waveforms with the same seismic signature. Although waveform cross-correlation can be fully automated and multiple events can be used, seismic computing limitations allowed only for manual waveform correlation. The seismic spectrum of an earthquake, say, F(t) = Ss(f) * Sp(f) * St(f), represents the earthquake source, the earthquake propagation, and the site response, respectively (Stein & Wysession, 2003). Given that the site response is constant, if two seismic waveforms have nearly identical seismic signatures, it can be assumed that both the area of fracture and the direction of wave propagation to a specific seismic station are the same.

After comparing different waveforms from earthquakes located within the Keck Network, four different earthquake clusters were identified, each with three similar earthquake events. The first cluster includes events that occurred on July 3 at 06:12 UTC and 09:03 UTC, and one event on July 5 at 05:38 UTC. Figure 25a shows the north and vertical components of the three

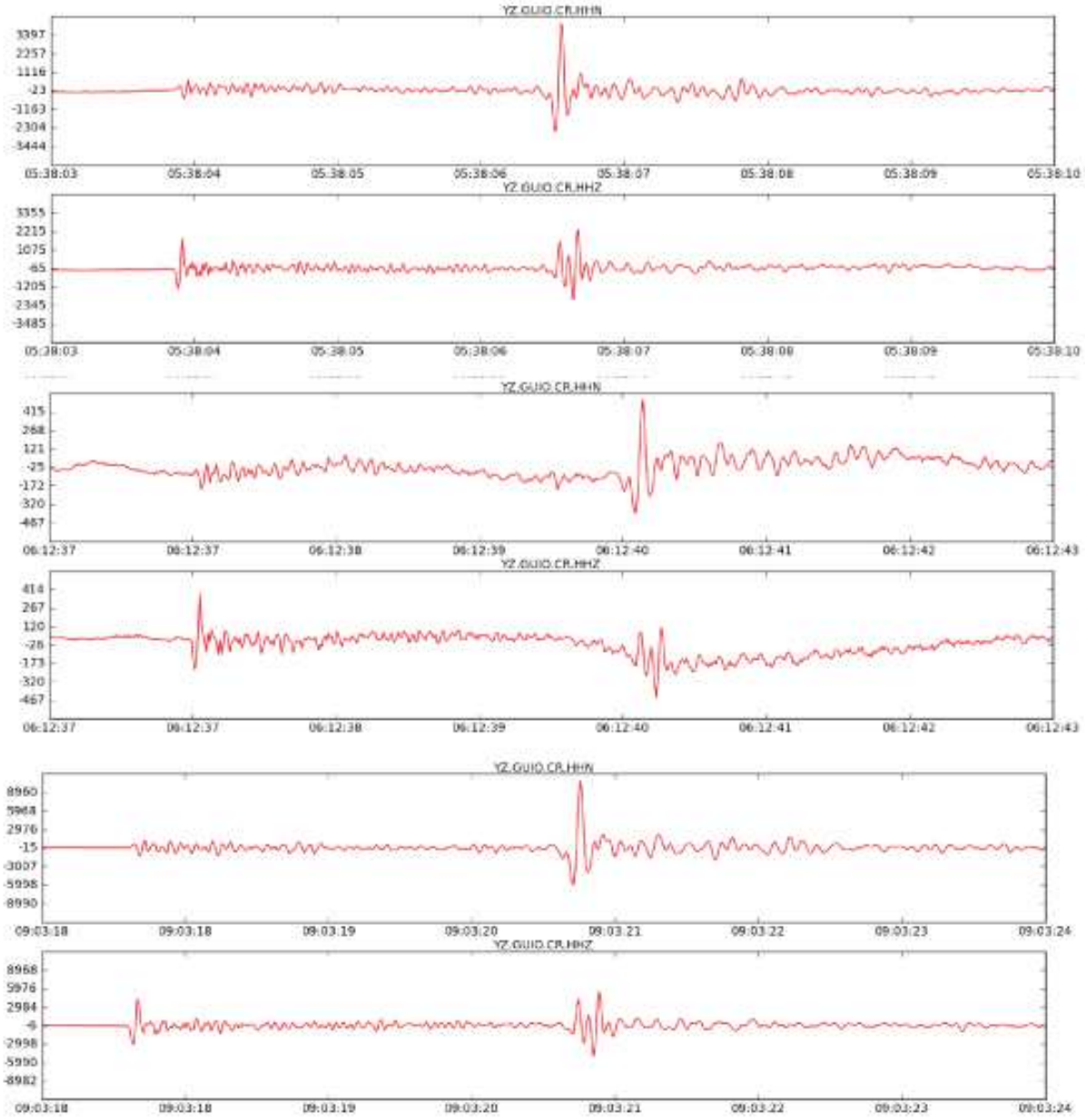

Figure 25a. Seismograms for the vertical (GUIO.CR.HHZ) and horizontal (GUIO.CR.HHN) components of three earthquakes, as recorded by the GUIO station at Playa Guiones. Notice the P-wave arrivals on the vertical stations and the S-wave arrivals on the horizontal-component stations exhibit the same seismic signature, with the S-wave arriving ~2.5s following the P-wave arrival.

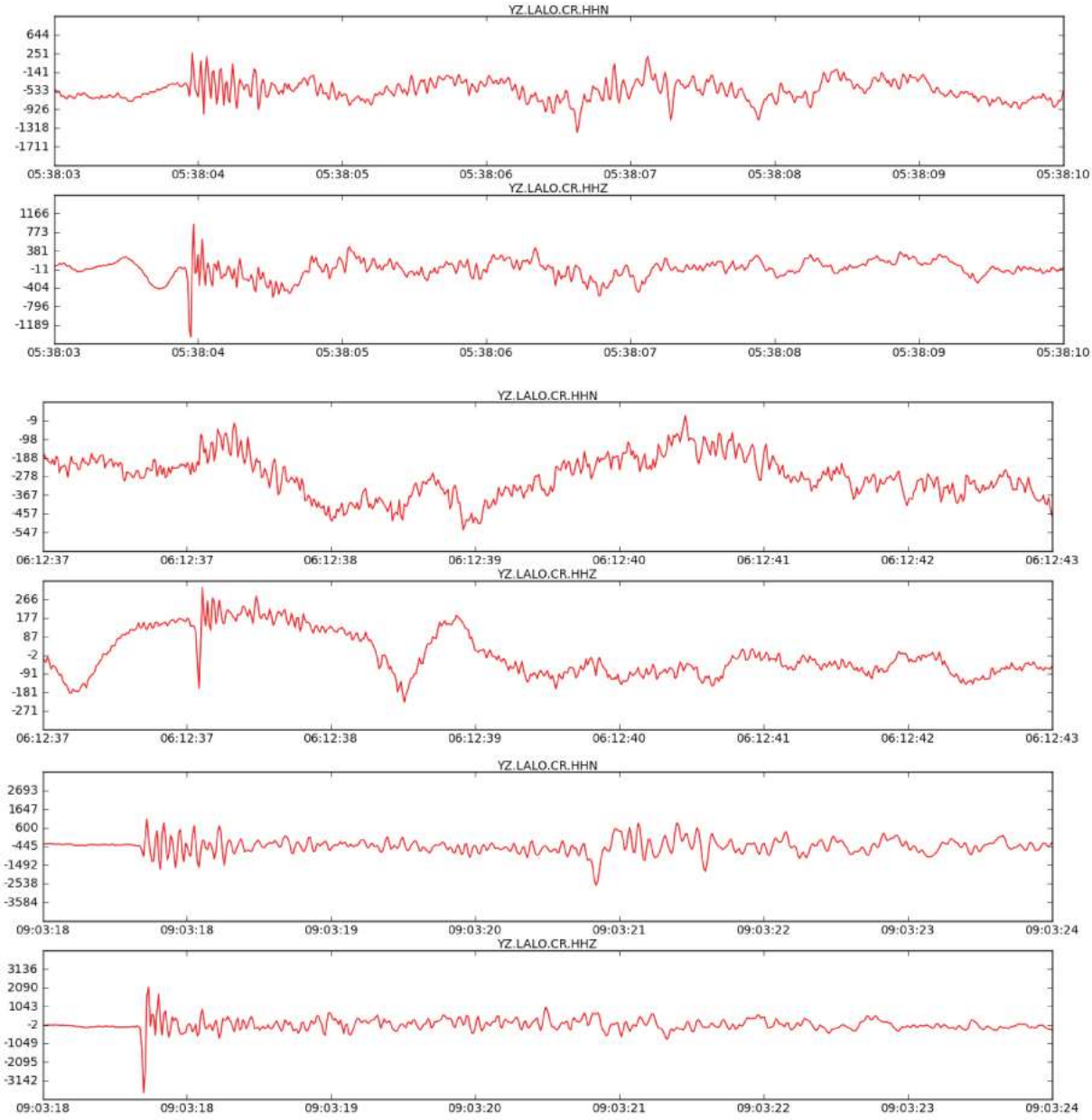

Figure 25b. Additional example of correlated waveforms recorded on the LALO Keck station. Each vertical component (YZ.LALO.CR.HHZ) is sharply dilatational, and on all three horizontal components, the S-wave arrives ~2.5s following the P-wave arrival. The LALO staiton exhibits a higher signal-to-noise ratio than the GUIO stations, which makes the S-wave arrival more difficult to identify.

separate earthquakes, as recorded by the GUIO station. Notice that on each vertical component of each earthquake, denoted by the header YZ.GUIO.CR.HHZ, all of the P-wave arrivals are down. Additionally, look at the three north-component traces, indicated by the header YZ.GUIO.CR.HHN. The S-wave arrival is clearly shown on each event by the increase in wave amplitude ~2.5 s following the initial P-wave arrival and is identical on all three traces. Because of the similar time differences between the P- and S- wave arrivals and the identical P-wave and S-wave arrivals at GUIO, it can be concluded that these earthquakes originated from the same source and propagated along the same path to the GUIO seismic station. The waveforms were also identical on the other 4 stations, with one more example of the correlated waveform shown at the LALO station (Figure 25b). Once again, notice the P-wave arrivals on the three Z components all show the same sharp, dilatational movement. Additionally, the S-wave arrivals on the three N components all show a small-amplitude dip in the S-wave arrival ~2.5 seconds following the P-wave arrival, the same time difference recorded at GUIO (Figure 25b).

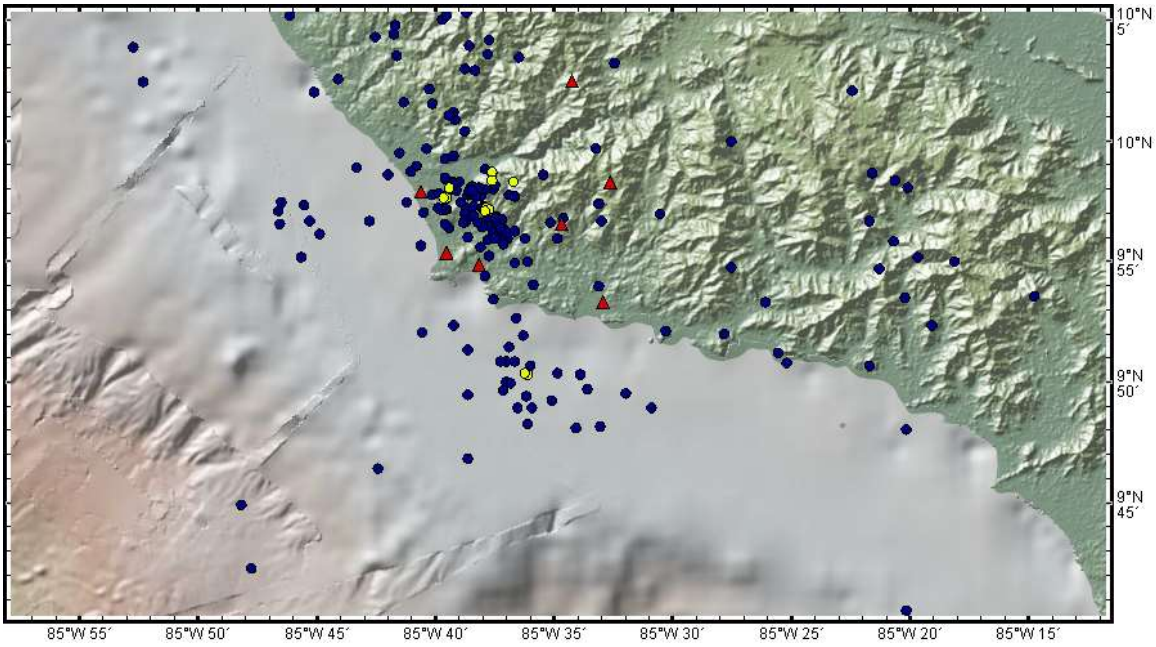

Figure 26. Earthquake locations represented by the blue dots, locally around the seismic stations (red triangles). The yellow locations represent the locations of the earthquake clusters with similar seismic signatures. Three clusters are located on-land, while one cluster is located offshore.

Three other clusters of correlated waveforms were identified in the data set, with each cluster containing three different earthquakes exhibiting similar seismic signatures, as identified by the yellow earthquakes in Figure 26.

Focal Mechanisms

Focal mechanisms were created for multiple events located using the Keck and Nicoya Networks, including the June 23rd aftershock. The Mw= 5.7 aftershock event exhibits pure thrust motion with a strike of 135º, and a dip of 60º (Figure 27). The multiple solutions shown in Figure Jz represent the precision of the Focmec program to reproduce very similar solutions, since 33 P-wave polarities were picked using Nicoya Network stations.

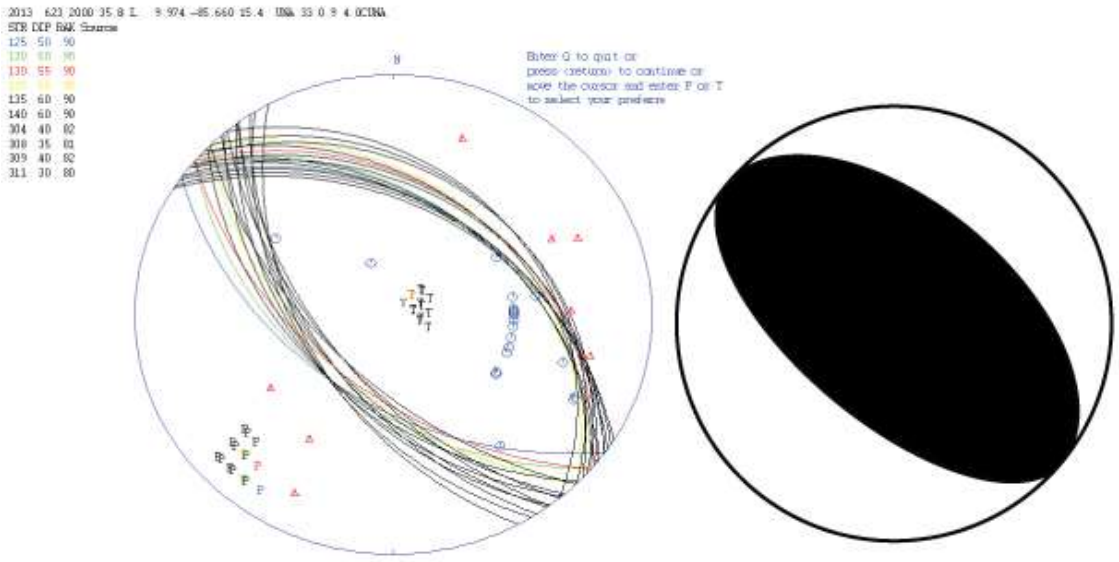

Figure 27. Raw focal mechanism (left) and corresponding beachball diagram (right). 33 P-wave polarities were used to compute this fault plane solution for the June 23, Mw=5.7 event, created by a thrusting event along a 50º dip and a trench-parallel strike.

Five of the twelve other earthquakes with calculated focal mechanisms exhibited thrust motion, including the June 24, July 3, July 5, July 6, and July 11 events (Figure 28). Each calculated thrust focal mechanism strikes to the northeast at an angle similar to that of the June 23 aftershock. Additionally, these thrust faulted earthquakes contain depths of 24.7 km, 21.3 km,

20.9 km, 16.3 km, and 18.4 km, respectively, with the epicentral locations shown in Figure 28b. An additional normal faulted earthquake on July 4 at 00:24 UTC that was not part of the correlated cluster previously identified, was located at ~18 km depth in the cluster of events offshore. Lastly, two anomalous focal mechanisms, the July 10, 18:31 event and the July 14, 16:51 UTC event exhibit oblique slip motion.

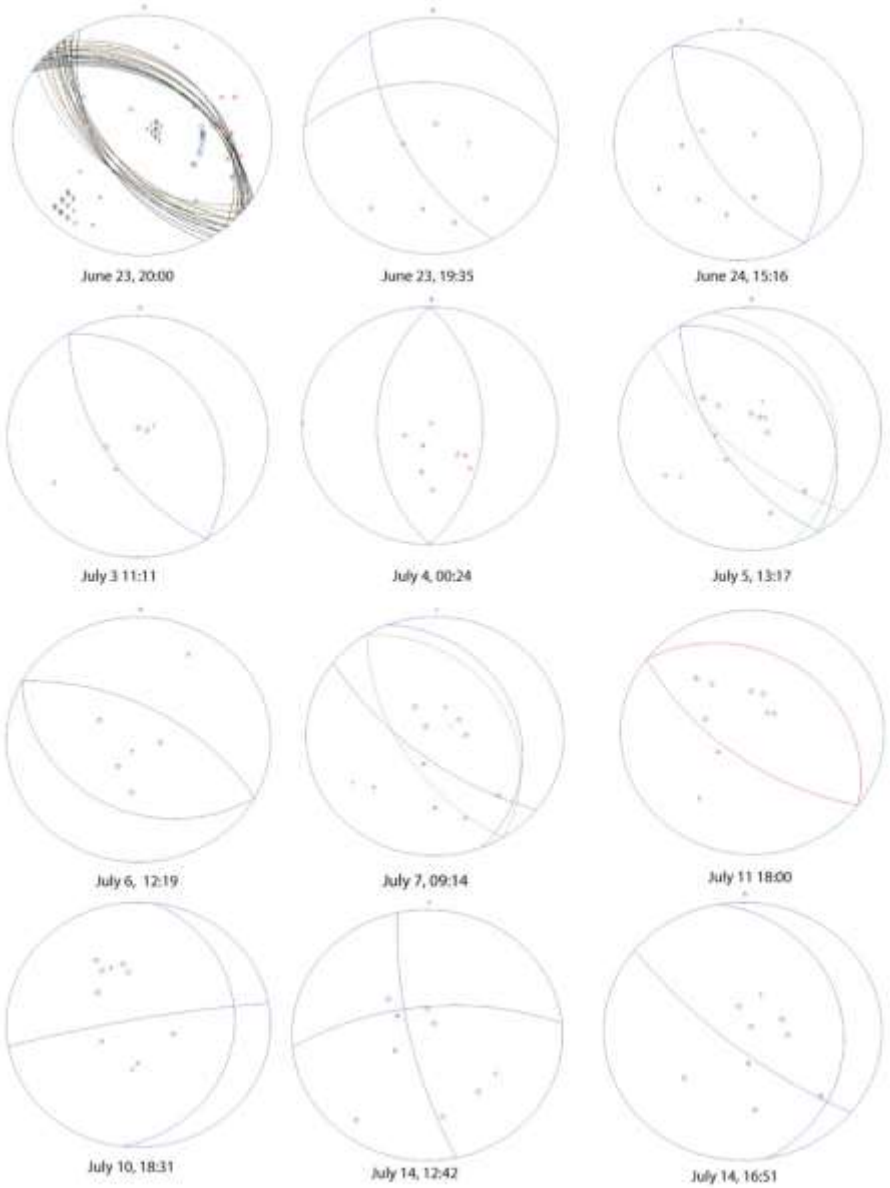

Figure 28. Raw focal mechanisms calculated using the FOCMEC program in Seisan, created from multiple events located around the KECK network. Blue circles represent seismic stations with compressional P-waves, and red triangles represent seismic stations with dilatational P-waves.

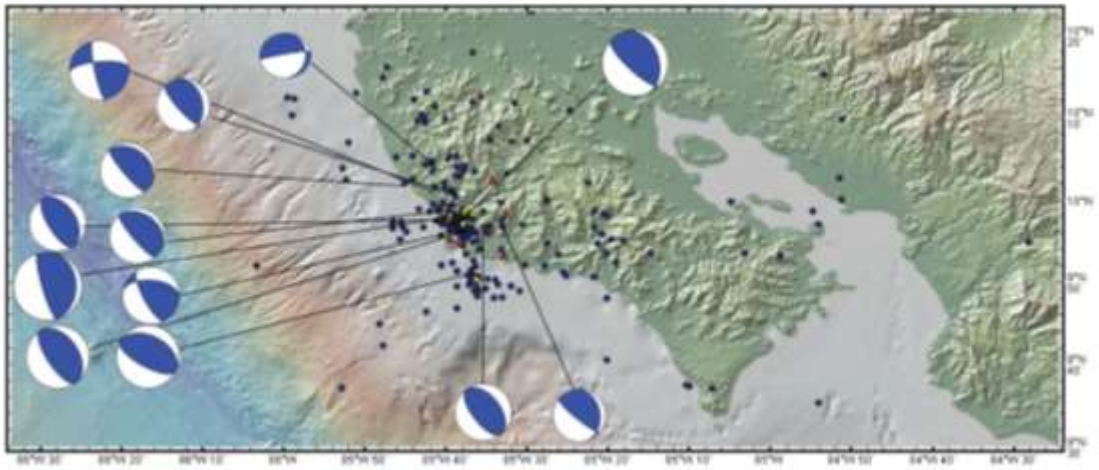

Figure 28b. Earthquake location map and corresponding focal mechanisms for multiple events around the Keck Network. Many of these single-event focal mechanisms exhibit shallow-dipping thrust faulting, with one event exhibiting strike-slip motion.

Composite Focal Mechanisms

Composite focal mechanisms were created from the single-event focal mechanisms created for the four event clusters (Figure 29). The first cluster, consisting of three normal faulting events, were combined to create a composite, normal-faulting focal mechanism with the angle of strike of the nodal plane oriented approximately parallel to the strike of the Middle America Trench. The second earthquake cluster, located to the southeast of the normal-faulted earthquakes, consisted of two strike-slip focal mechanisms and one shallow-dipping single-event focal mechanism. Combining the three events together, a composite, shallow dipping thrust event was created. The last cluster further inland also consisted of two strike slip fault plane solutions and one normal faulting fault plane solution, and the composite strike-slip fault plane solution was created from those single-event mechanisms. Lastly, a cluster of events offshore consisted of two thrusting fault plane solutions and one strike-slip solution, with the composite solution exhibiting shallow-dipping thrust motion (Figure 29).

The raw-data focal mechanisms from Seisan and the correlated composite focal mechanism for the four clustered events are shown in Figure 30. In the first cluster of events, it is evident that there exists dilatation on all stations for each event, directly in the center of each

stereonet, which leads to the composite focal mechanism of pure normal motion with the fault plane oriented parallel to the strike of the Middle America Trench. For the second cluster of events, while strike slip motion is seen on the two June 24 events, a fault plane solution that fits all of the single-event mechanisms is a thrusting event. Lastly, combining the three single-event focal mechanisms into one composite focal mechanism yields the composite thrusting and strike-slip mechanism in cluster 3 and cluster 4, respectively.

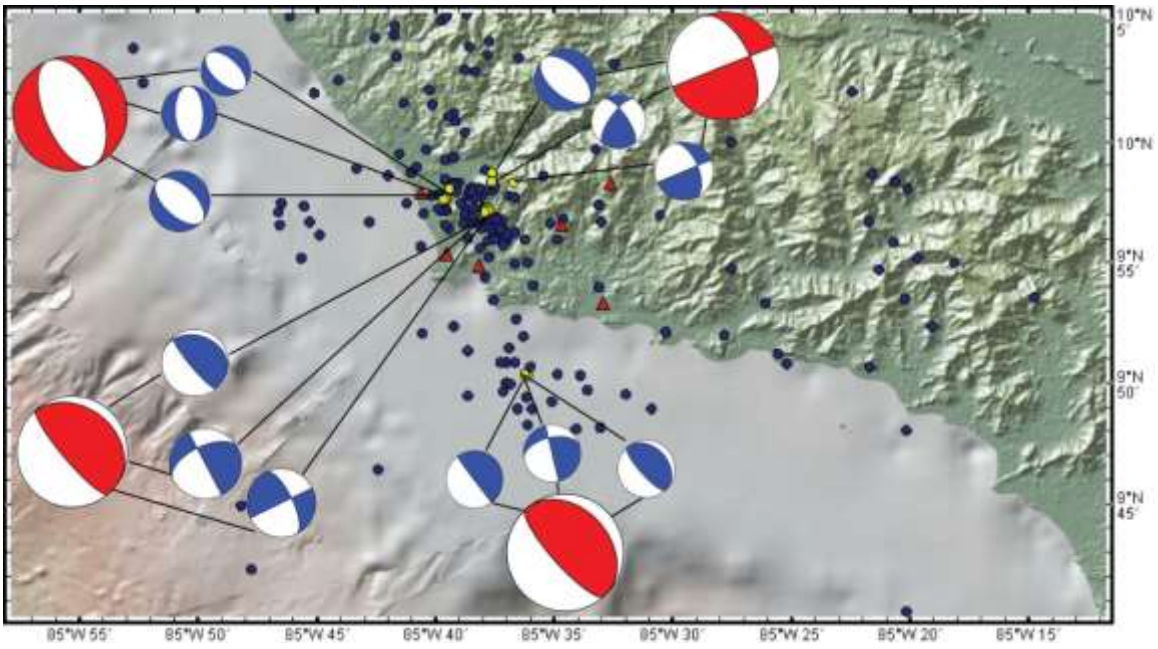

Figure 29. Composite focal mechanisms (red) interpreted from the single-event focal mechanisms (blue). For each earthquake cluster, three single-event focal mechanisms were analyzed to produce the composite focal mechanism. One cluster exhibited normal motion, two clusters exhibited thrust motion, and one other cluster exhibited strike-slip motion.

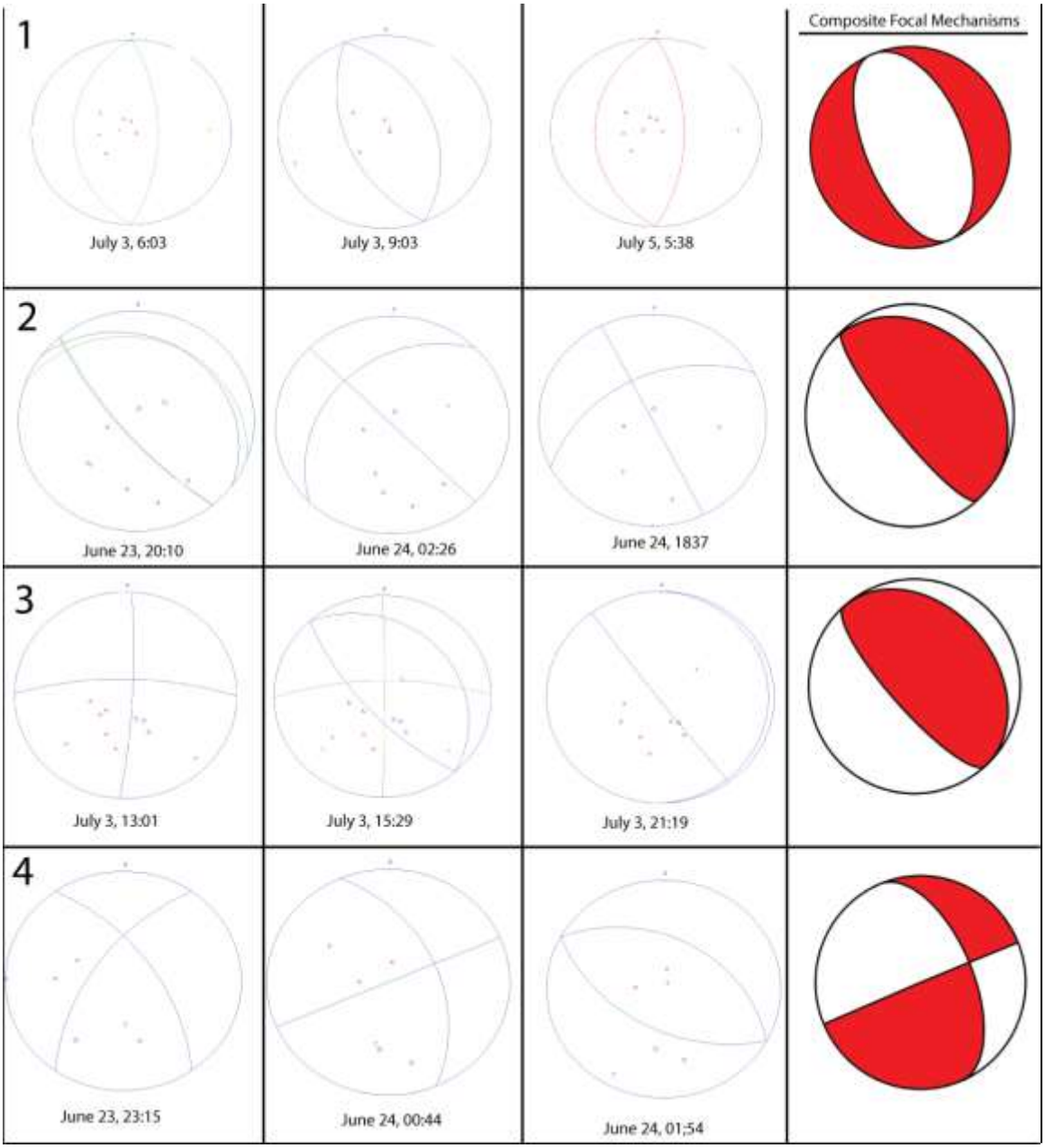

Figure 30. Raw single-event focal mechanisms created using FOCMEC, and the correlated focal mechanism in red. The correlated focal mechanisms were interpreted from the single-event station data and are assumed to be more accurate representations of the earthquake faulting. It's evident that while some single-event focal mechanisms exhibited strike-slip motion, such as what is shown in cluster 2, using data from other events affirms a thrusting event rather than a strike-slip event.

DISCUSSION

The June 23rd, M_w= 5.7 Event

The June 23rd, M_w= 5.7 earthquake represents an aftershock of the September 5, 2012 M_w=7.6 Nicoya earthquake that ruptured the onland section of the locked region of the plate interface between the subducting Cocos plate and the overriding Caribbean plate (Protti et al., 2014). The fault plane solution calculated for this event dips at 50º (Figure 27), and is oriented parallel to the strike of the Middle America Trench. Exhibiting thrusting motion, this aftershock was most likely the result of underthrusting along the plate interface: the same process that has contributed to the past large earthquakes off the coast of Costa Rica in 1950 (M_s 7.7), 1978 (M_s 7.0), 1990 (M_w 7.0), and most recently in 2012 (M_w 7.6) (Avants et al., 2001).

While the 5 September, 2012 earthquake initiated offshore, as shown in previous figures, the area of rupture occurred primarily beneath the Nicoya Peninsula. Thus, it is possible that this June 23rd event ruptured a small area along the plate interface that did not fully rupture in September. Additionally, the increase in seismicity on June 23 and June 24 following the June 23rd, 20:50 UTC event most likely represents very small patches of rupture around the main rupture area of the M_w= 5.7 event . These earthquakes yielded focal depths of 20.9 ± 5.7 km, the approximate depth of the plate interface beneath the Nicoya Peninsula. A depth of ~20 km also places the focal depths of these events within the boundary of plate interface microseismicity, 17-28 km beneath the northern Nicoya Peninsula, as defined by DeShon et al., (2006). Thus, it can be assumed that both the June 23rd M_w = 5.7 earthquake and its subsequent aftershocks represent small areas of rupture beneath the Nicoya Peninsula, along the plate interface that did not fully release the accumulated strain during the September 5, 2012 earthquake.

Earthquake Analysis

As previously stated, 254 events were recorded from June 23rd to July 18th, recorded by both the Nicoya Network and Keck Network. 191 of those 254 events were located between 16 and 24 km, which places them at the approximate depth of the plate interface. These events were

overlain onto past CRSEIZE data and a believed subducting plate interface beneath the Keck Network (DeShon et al., 2006, Figure 31). The earthquakes from these two experiments plot at very similar locations along the plate interface, with most of the earthquakes located along the plate interface, but there is also outlying seismicity located both in the overlying Caribbean plate and the subducting Cocos plate.

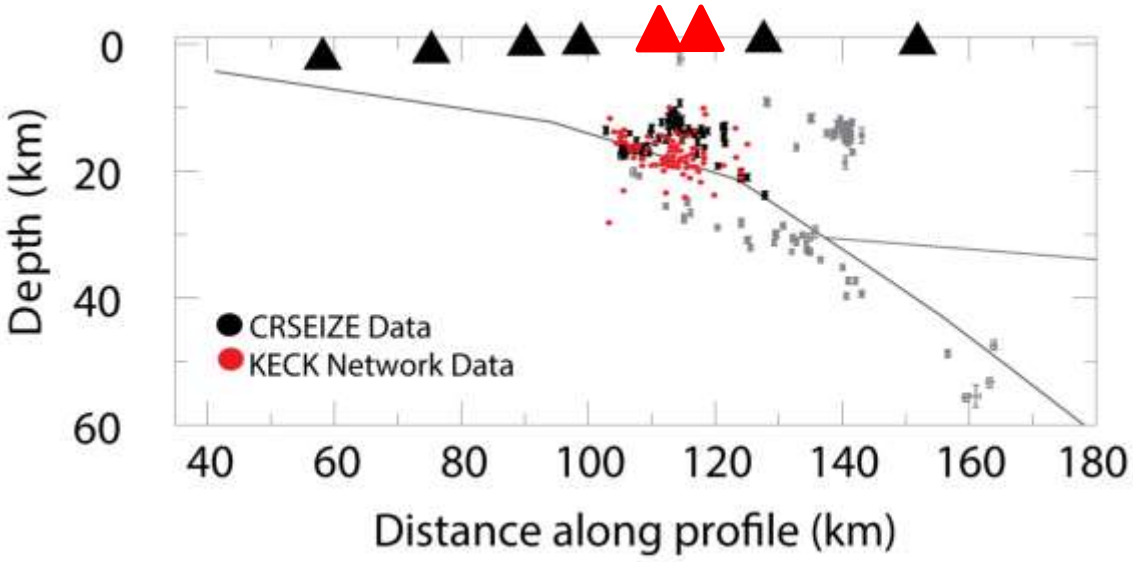

Figure 31. Seismic data locally around the Keck Network, overlying CRSEIZE data from beneath the Keck Network (DeShon et al., 2006). Notice the Keck Network data exhibits similar trends to the CRSEIZE data, with seismicity between 16 and 24 km depth. The triangles on the top represent seismic stations from the CRSEIZE experiment, with the triangle furthest left located at the outer rise, adjacent to the Middle America Trench.

The majority of the earthquakes located were within the area of interseismic coupling on the Nicoya Peninsula, as shown by the white area in Figure 32. The area of interseismic coupling, determined by Feng et al., (2012) represents the area of fully-coupled locking along the subducting plate interface that had accumulated since the last M>7 event in 1950. Yue et al., (2013) determined the coseismic rupture area 30 seconds following the mainshock, as outlined in blue, and additional coseismic rupture during the 2 weeks following the earthquake, represented by the red area, was determined by Protti et al., (2014). It's apparent that most of the seismicity between June 23 and July 18 is not located within the area of coseismic rupture, but rather just to

the west. The earthquakes from June 23 and June 24 are separate from the rest of the seismicity, and an estimated rupture area was created by outlining the spatial distribution of this seismicity (Figure 33). Fittingly, the June 23 event and its associated aftershocks are located adjacent to the coseismic rupture area of the September 5 event and located within the area of interseismic coupling, meaning that these events rupture an area of the plate interface that did not fully slip during the 2012 earthquake. Outlying earthquakes, located significantly outside of the network, were included in the overall earthquake database. However, due to the dense but localized nature of the Keck Network the epicentral and focal uncertainties for these earthquakes and were greater, so no further analysis was performed for these events.

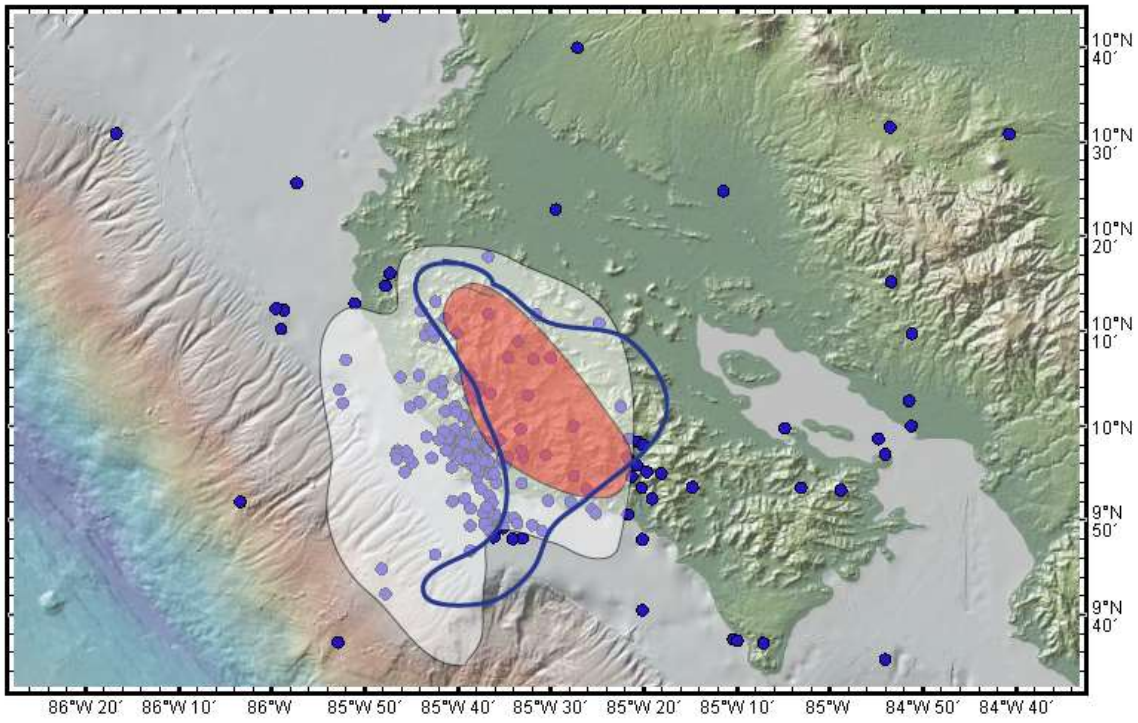

Figure 32. Seismicity recorded from June 23 to July 18 on the Nicoya Peninsula, overlain by the relative area of interseismic coupling (white), coseismic rupture 40 seconds following the Mw= 7.6 event (blue line), and additional coseismic rupture 2 weeks following the event (red). Most seismicity is located within the area of interseismic coupling and west of the area of coseismic rupture two weeks following the September 5, 2012 event.

Figure 33. Estimated coseismic rupture model created from the June 23 and June 24 aftershocks following the June 23 M_w= 5.7 event (in red). This area of rupture is adjacent to the coseismic rupture area following the September 5 earthquake and within the area of interseismic coupling determined from prior GPS studies.

Earthquake Depth Differences

The earthquakes captured by the Keck Network (Figure 24) exhibit changes in focal depths from north to south. Newman et al., (2002) performed seismic studies directly beneath the Nicoya Peninsula as part of the CRSEIZE experiment, in which hundreds of earthquake depths were determined. They showed that the updip limit of the seismogenic zone transitions from 20 km depth in the north to 10 km depth in the south. This difference in the seismogenic updip limit beneath the Nicoya Peninsula is attributed to the temperature difference between the subducting East Pacific Rise crust (north) and the Cocos-Nazca Spreading center (CNS) crust to the south (Newman et al., 2002).

Crustal temperature plays an important role in constraining the depth of seismicity along the plate interface. Dehydration reactions occur along the plate interface as it is heated at depth, which alters the plate interactions along the subducting interface from stable sliding to stick-slip sliding (Newman et al., 2002). The EPR-derived crust, which is both colder and older than the younger, warmer CNS crust, experiences these dehydration reactions deeper along the subduction

interface than the CNS crust. A temperature of 100-150ºC, which has been determined to be the temperature at which stable sliding turns into stick-slip sliding along the Middle America Trench (Hyndman and Wang, 1993), occurs at shallower depths along the plate interface for the subducting CNS crust than the subducting EPR crust due to its warmer thermal characteristics, influencing the depth at which this seismicity begins.

This transition in earthquake hypocenter depth from north to south is clearly represented in the data locally around the Keck network, as identified by the two yellow circles in Figure 34. The cluster of earthquakes onshore and to the north, which predominantly have calculated depths of ~20 km, are deeper than the cluster of events offshore, which predominantly have depths of ~15 km. Notice that the EPR/CNS divide reaches the Nicoya Peninsula directly at the elbow of the peninsula, separating the northern cluster and southern cluster. Thus the thermal states of the EPR-derived crust and the CNS-derived crust affect where the seismicity is occurring and the focal depths of these events. It is interesting to note, however, that seismicity is absent both offshore on the EPR subducting crust and onshore on the CNS subducting crust; areas that may represent already ruptured areas along the subducting interface, or areas yet to be ruptured.

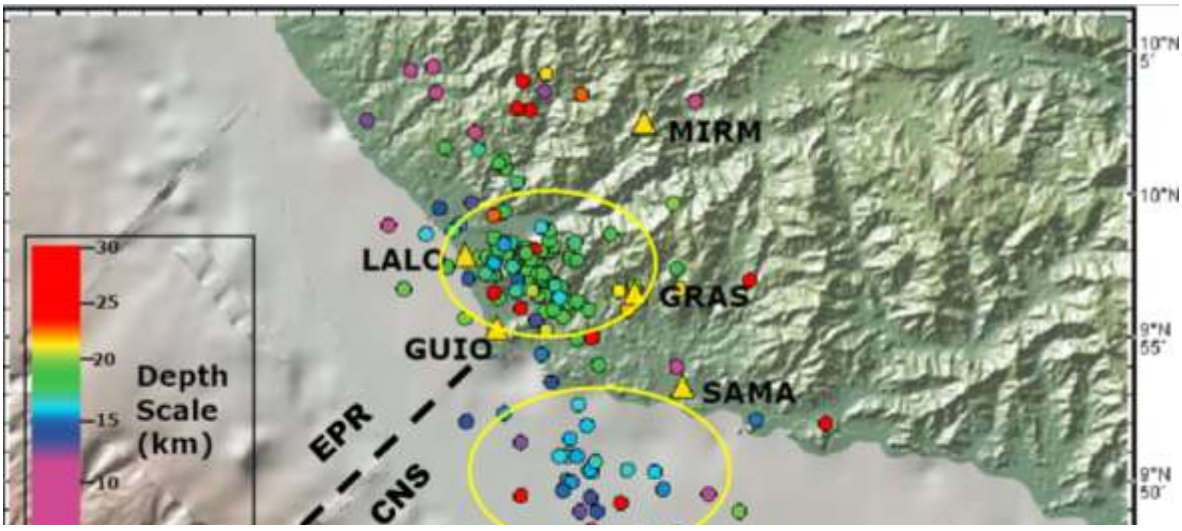

Figure 34. Similar to Figure Gz, but with added yellow circles around two distinct earthquake clusters, and the EPR-CNS boundary as it reaches the coast of the Nicoya Peninsula. The cluster to the north, influenced by the colder EPR-derived crust, contains focal depths of ~20 km, while the warmer CNS-derived crust causes a decrease in seismicity depth, to ~15 km in the southern cluster.

This means that this seismic network has detected where seismicity has dominated at depth along the plate interface, which varies from north to south (Figure 34), but this lack of seismicity both on shore and offshore makes it difficult to constrain the updip and downdip changes in focal depth on the EPR crust versus the CNS crust.

Intraplate Seismicity

Multiple events greater than 24 km that are located within the Keck Network, as indicated by the red circles in Figure 34, represent intraplate earthquakes originating within the subducting Cocos slab. A single focal mechanism calculated for an event at 24 km depth on July 10 at 18:31 UTC exhibited oblique slip motion. This fault plane solution is most like not very accurate, because even though the depth of the event is well constrained, it was located to the north of the network where station coverage is lacking. Thus, even though this earthquake exhibits oblique slip, and because this earthquake does not occur near the localized Keck network, the calculated focal mechanism would benefit from more stations.

Events shallower than 15 km, which are scattered around the Keck network and indicated by purple circles in Figure 34, either represent shallow intraplate earthquakes, or there exists error associated with the location. Previous focal mechanism studies on the overlying crust on the Nicoya Peninsula have identified pure strike-slip events with a north-west-striking nodal plane, parallel to the MAT (Hansen et al., 2006). One calculated strike-slip focal mechanism, as shown in Figure 35, contains a slightly northwest-striking nodal plane with right-lateral motion. While strike-slip motion would typically be evident on the overriding plate, this event is located at 21.2 km depth, which places the earthquake very close to the plate interface. This strike-slip motion is likely the result of Cocos-Caribbean oblique convergence, which occurs along this subduction interface (Feng et al., 2012). Better depth constraints are needed to determine whether this earthquake formed on a shallow crustal fault, but there existed limitations in the number of stations used to determine focal depths.

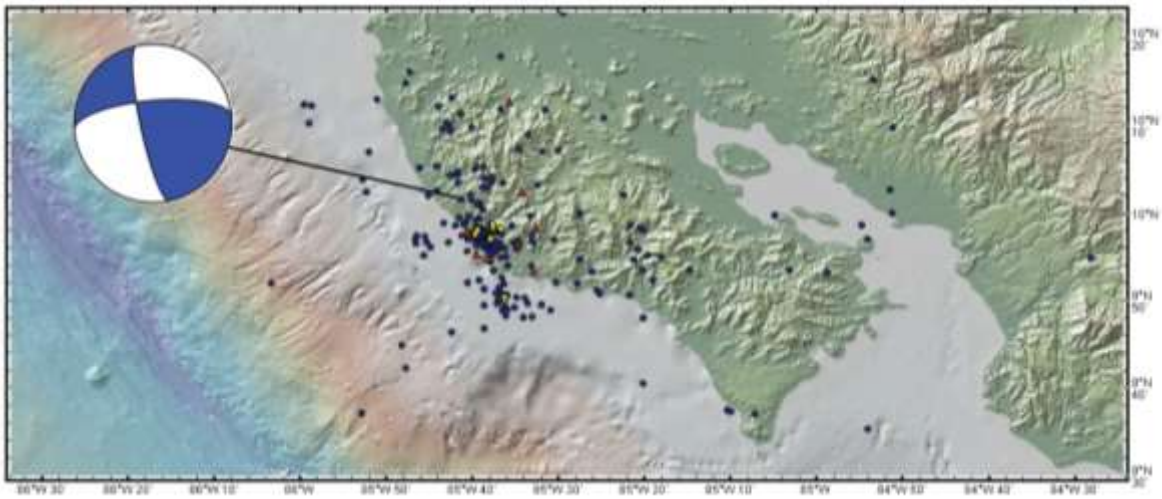

Figure 35. Strike-slip fault plane solution with a nodal plane dipping slightly northwest to the Middle America Trench. This event, located at 21.2 km, possibly represents a deep, intraplate event in the overlying Caribbean plate, in which there exists Cocos-Caribbean oblique convergence as determined by GPS measurements (Feng et al., 2012).

Interplate Seismicity

The vast majority of the seismicity recorded by the Keck Network is located along the plate interface, at 16-24 km depth, which is expected since the Nicoya Peninsula lies directly above the seismogenic zone in this subduction environment. Focal mechanisms were computed for both single events and earthquake clusters along the interface, and it's apparent that the dominant faulting mechanism creating these earthquakes is thrust motion. Thrusting fault plane solutions have been calculated along the entire seismogenic zone, from 16.3 km to 24.7 km, which indicates that underthrusting occurs along the entire subduction zone. Additionally, the strikes of these thrusting events are oriented to the northwest, parallel to sub-parallel to the angle of strike of the Middle America Trench. Dips of these thrust events ranged from 16º to 60º, a wide range of dipping angles due to the lack of the number of stations used.

Previous focal mechanism studies have linked the EPR/CNS subducting lithospheres to different layers of underthrusting beneath the Nicoya Peninsula (Hansen et al., 2006), in which two distinct layers of underthrusting are formed from this crustal temperature difference and affect the updip limit of seismicity along this subduction zone. This hypothesis can be affirmed

by the Keck Network data, in which the offshore single-event clusters and the respective composite focal mechanism (Figure 29), have depths of ~17-18 km, while the other thrust events contain depths of ~20 km and deeper. These small-magnitude thrust events, which exhibit northeasterly dipping nodal planes consistent with the subduction of the Cocos Plate, serve as a useful reminder of the active seismicity that has the potential to produce large, damaging earthquakes.

Peculiar Normal Faulting

Following waveform correlation and the identification of clusters, the normal faulting cluster of events (Figure 29) represents anomalous faulting along the seismogenic zone beneath the Nicoya Peninsula that is uncharacteristic downdip from the trench. Typically, normal faulting earthquakes occur along the outer-rise (Figure 36), in a tensional environment where the subducting slab bends and consequently flexes. Extensional normal faults occur, which can produce significant offshore earthquakes. The last outer rise earthquake off the coast of the Nicoya Peninsula, a Mw= 6.4 event on July 21, 2000. The normal faulting events observed in this study, however, are located ~60 km away from the Middle America Trench and cannot be classified as an outer rise event.

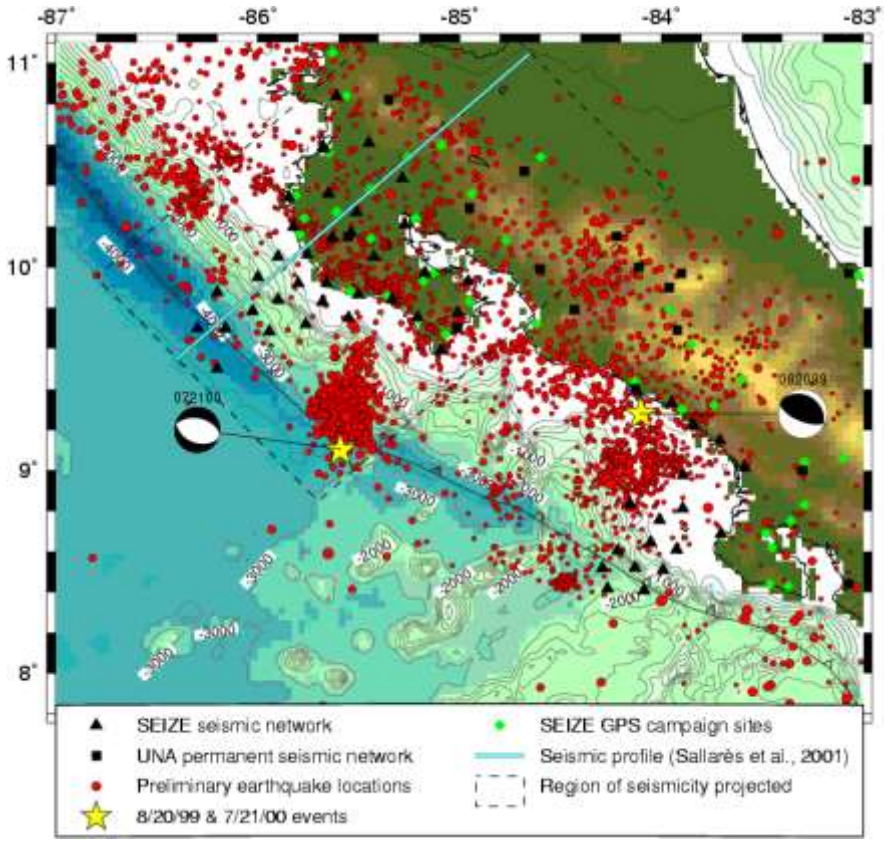

Figure 36. An outer rise event off the coast of the Nicoya Peninsula, on July 21, 2000. This outer rise event exhibits normal faulting motion, and was a magnitude 6.4 event that was created due to the flexure and bending of the Cocos plate subducting beneath the Caribbean plate, creating extensional normal faults seaward of the Middle America Trench.

Because the cluster of normal faulting events occurred ~60 km from the trench, and have focal depths of ~19-20 km, these earthquakes occurred very close to the subducting plate interface. These normal faulting earthquakes most like do not originate in the overlying Caribbean plate, because at that depth, the Caribbean plate is experiencing compression and therefore normal faulting would not be created. These earthquakes most likely did not originate along the plate interface where underthrusting is the dominant process. Thus, the one plausible origin for these earthquakes is in the Cocos Plate, beneath the subducting plate interface.

Figure 37 highlights the extensional environment that forms at the outer rise, as shown by the bathymetry to the left of the Middle America Trench. These normal faults that formed at the outer rise are extremely important, because the normal faulting that occurred beneath the Nicoya

Peninsula could represent reactivated normal faults that formed at the surface, adjacent to the Middle America Trench. As oceanic plates such as the Cocos plate subduct and normal faults are created at the outer rise, fluids are introduced into the lithospheres which are then subducted in the pores of the subducting rock. As these normal faults get deeper into the subduction zone, metamorphic processes can release fluids in the downgoing plate, which can promote brittle failure along preexisting faults (Ranero et al., 2003).

This hypothesis can be strengthened if more P-wave polarities were plotted on the stereonet. While it is apparent that these earthquakes are not thrust events, considering dilatational movement plots in the center of the stereonet, it is possible that these events are intraplate strike-slip events. Additionally, the lack of a larger seismic network can contribute to greater depth errors for these earthquakes. Regardless, discovering this evidence of normal faulting at the upper extent of the subducting Cocos plate is important for characterizing the various types of active seismicity along the seismogenic zone beneath the Nicoya Peninsula.

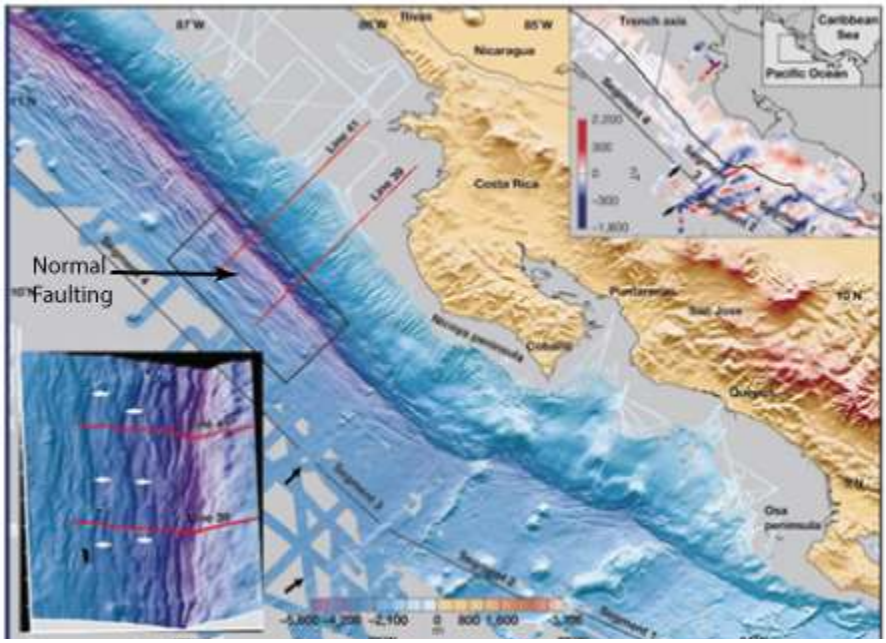

Figure 37. Bathymetry off the coast of the Nicoya Peninsula, specifically along the outer rise. Notice the normal faulting that forms from the bending of the Cocos plate beneath the Caribbean plate along the Middle America Trench (Ranero et al., 2003).

CONCLUSIONS

The Nicoya Peninsula has provided a unique environment to monitor active seismicity directly above the seismogenic zone of the subducting plate interface beneath Costa Rica. After deploying a five station seismic network above the area of rupture 10 months following the M_w = 7.6 Nicoya Earthquake on September 5, 2012, interesting interpretations can be made with 3.5 weeks of seismic data. Firstly, the M_w= 5.7 earthquake on June 23, 2013, an aftershock of the September 5 event, ruptured an area of the plate interface that had accumulated strain since the last earthquake in 1950, but did not fully rupture in September. The known difference in earthquake depths from the north to south along the Nicoya Peninsula is exemplified in the data collected by the Keck Network, providing support for the EPR/CNS crustal temperature variation and its effect on the depth of seismicity. Much of the seismicity recorded from June 23 to July 18 was located along the seismogenic zone of the subducting plate interface, with focal mechanism analysis showing predominantly thrust motion along the plate interface, resulting from underthrusting of the Cocos Plate beneath the Caribbean Plate. Additionally, there is evidence of normal faulting motion beneath the plate interface, formed from the reactivation of normal faults that formed at the outer rise.

Even though this seismic study is smaller than other studies performed on the Nicoya Peninsula, these conclusions are important for characterizing the seismicity that occurs in an area of high seismic risk. Following the M_w= 7.6 earthquake in September of 2012, it has been determined that there exists a significant area along the plate interface that had accumulated seismic strain since the last M>7 earthquake in 1950, but did not rupture during the September 5th event. Thus, the entire Nicoya Seismic gap has not been filled, and there still exists a remaining locked patch offshore of the Nicoya Peninsula that has the potential to generate an earthquake up to M_w= 6.9 (Protti et al., 2014). While these earthquake events cannot be avoided, it is our duty to understand the seismic cycle in these areas prone to megathrust events, and to educate citizens about an earthquake's deadly nature, in hopes ultimately save lives when the moment arrives.

REFERENCES

Avants, M., Schwartz, S.Y., Newman, A., DeShon, H.R., Protti, M., Guendel, F., 2001, Large Underthrusting Earthquakes Beneath the Nicoya Peninsula, Costa Rica: Eos Trans. AGU, Fall Meet. Suppl., T52E-07.

Bilek, S.L., Schwartz, S.Y., and DeShon, H.R., 2003, Control of seafloor roughness on earthquake rupture behavior: Geology, v. 31, p. 455-458.

Barkhausen, U., Ranero, C.R., von Huene, R., Cande, S.C. & Roeser, H.A., 2001, Revised tectonic boundaries in the Cocos plate off Costa Rica: implications for the segmentation of the convergent margin and for plate tectonic models: J, Geophys. Res., v. 106, 19 207-19 220.

DeShon, H.R., Schwartz,S.Y, Newman, A.V., González, V., Protti, M., Dorman, L.M. Dixon, T.H., Sampson,D.E., Flueh, E.R., 2006, Seismogenic zone structure beneath the Nicoya Peninsula, Costa Rica, from three-dimensional local earthquake P- and S-wave tomography: Geophys. J. International, v. 164, p. 109-124.

Dixon, T. H., "GPS & Seismic Studies of Episodic Tremor and Slip on the Nicoya Peninsula, Costa Rica". Powerpoint Presentation. MARGINS Lecturer. February/March 2009.

Feng, L., Newman, A.V., Protti, M., González, V., Jiang, Y, Dixon, T.H., 2012, Active deformation near the Nicoya Peninsula, northwestern Costa Rica, between 1996 and 2010: Interseismic megathrust coupling: J. Geophys. Res., v. 117, B0647, p. 1-23.

Fisher, R.L. 1961, Middle America Trench – Topography and Structure: Geol. Soc. Am. Bull., v. 72, p. 703-720.

Hansen, S.E., Schwartz, S.Y., DeShon, H.R., and González, V, 2006, Earthquake relocation and focal mechanism determination using waveform cross correlation, Nicoya Peninsula, Costa Rica: Bull. Seism. Soc. Am., V. 96, no. 3, pp. 1003-1011.

Haskov, J., and Ottemöller, L, 1999, SeisAn Earthquake analysis software: Seismological Research Letters, v. 70.

Hyndman, R.D., Wang, K., 1993, Thermal constraints on the zone of possible major thrust earthquake failure on the Cascadia Margin: J. Geophys. Res., v. 98, p. 2039-2060.

Kennett, B.L.N., and Engdahl, E.R., 1991, Traveltimes for global earthquake location and phase identification: Geophys. J. International, v. 122, p. 178-184.

Marshall, J.S. & Anderson, R.S., 1995, Quaternary uplift and seismic cycle deformation, Peninsula de Nicoya, Costa Rica: Geol. Soc. Am. Bull., v. 107, p. 463-473.

Newman, A.V., Schwartz, S.Y., González, V., DeShon, H.R., Protti, M., Dorman, L.M., 2002, Along-strike variability in the seismogenic zone below Nicoya Peinsula, Costa Rica: Geophys. Res. Let., v. 29, no. 20, p. 1-4.

Pacheco, J.F., and Sykes, L., 1992, Changes in frequency-size relationship from small to large earthquakes: Nature, v. 355, p. 71-73.

Protti, M., McNally, K., Pacheco, J., González, V., Montero, C., Segura, J., Brenes, J., Barboza, V., Malavassi, E., Güendel, F., Simila, G., Rojas, D., Velasco, A., Mata, A., Schillinger, W., 1995, The March 25, 1990 (M_w=7.0, M_L=6.8) earthquake at the entrance of the Nicoya Gulf, Costa Rica: Its prior activity, foreshocks, aftershocks, and triggered seismicity. J. Geophys. Res., v. 100, p. 20345-20358.

Protti, M., González, V, Newman, A.V., Dixon, T.H., Schwartz, S.Y., Marshall, J.S., Feng, L., Walter, J.L., Malservisi, R., Owen, S.E., 2014, Nicoya earthquake rupture anticipated by geodetic measurement of the locked plate interface: Nature Geoscience, v. 7, p. 117-121.

Ranero, C.R., Phipps, M.J., McIntosh, K., Reichert, C., 2003, Bending-related faulting and mantle serpentinization at the Middle America Trench: Nature, v. 425, p. 367-373.

Ranero, C., Grevemeyer, I., Sahling, H., Barckhausen, U., Hensen, C., Wallmann, K., Weinrebe, W., Vannucchi, P., von Huene, R., and McIntosh, K., 2008, The hydrogeological system of erosional convergent margins and its influence on tectonics and interplate seismogenesis: Geochem., Geophys., Geosyst., v. 9, p. Q03504.

Stein, S. & Wysession, M., 2003, An Introduction to Seismology, Earthquakes, and Earth Structure, Blackwell Publishing, Oxford, 498 pp., ISBN 0-86542-078-5.

Yue, H., Lay, T., Schwartz, S.Y., Rivera, L., Protti, M., Dixon, T., Owen,S., Newman, A.V., 2013, The 5 September 2012 Nicoya, Costa Rica M_w 7.6 earthquake rupture process from joint inversion of high-rate GPS, strong-motion, and teleseismic P wave data and its relationship to adjacent plate boundary interface properties: J. Geophys. Res.., v. 118, p. 1-14.

Appendix

HOUR	DATE	Time	Seconds	Latitude	Longitude	Depth	Picks	RMS	Magnitude
2013	623	223	1.8	10.117	-85.867	25.1	3	0.1	0.9CUNA
2013	623	1921	37.1	9.801	-85.336	22.8	5	1.1	2.0CUNA
2013	623	1927	26.5	10.15	-85.559	31.3	3	0	1.1CUNA
2013	623	1935	12.3	9.948	-85.624	20.9	5	0	1.6CUNA
2013	623	2000	35.8	9.974	-85.66	15.4	33	0.9	4.0CUNA
2013	623	2010	50.6	9.953	-85.629	20.4	4	0	1.4CUNA
2013	623	2020	10.9	9.967	-85.626	20	3	0	0.7CUNA
2013	623	2021	29.2	9.963	-85.669	21.1	3	0.1	1.2CUNA
2013	623	2023	31.8	9.962	-85.635	20.9	3	0	1.1CUNA
2013	623	2027	36.2	9.954	-85.645	20.8	3	0	0.8CUNA
2013	623	2033	20.9	9.97	-85.625	20.8	3	0	0.9CUNA
2013	623	2033	44.9	9.934	-85.644	26.3	3	0.5	1.2CUNA
2013	623	2035	11.9	9.933	-85.616	19.8	3	0	1.0CUNA
2013	623	2044	25.2	9.967	-85.632	21	4	0	1.3CUNA
2013	623	2050	56.4	10.034	-85.752	2.8	4	1.1	1.4CUNA
2013	623	2102	34.5	9.966	-85.652	19.5	3	0	0.9CUNA
2013	623	2105	32.8	9.954	-85.634	19.6	3	0	0.9CUNA
2013	623	2107	29	9.937	-85.626	20.2	3	0	0.7CUNA
2013	623	2117	50.1	9.938	-85.626	19.5	3	0	0.7CUNA
2013	623	2118	26.1	10.058	-85.608	23.6	3	0.1	0.7CUNA
2013	623	2132	41.5	9.963	-85.644	19.5	3	0	0.6CUNA
2013	623	2141	37.1	9.933	-85.581	23	4	0.3	1.2CUNA
2013	623	2146	23.8	9.955	-85.633	20.3	3	0	0.9CUNA
2013	623	2159	6.5	9.943	-85.632	20	3	0	0.7CUNA
2013	623	2204	54.2	9.946	-85.63	20.5	3	0	0.9CUNA
2013	623	2214	42.4	9.935	-85.623	19.8	4	0	1.0CUNA
2013	623	2215	59.4	9.944	-85.633	20	3	0	0.8CUNA
2013	623	2216	45	9.907	-85.632	17.3	3	0	0.8CUNA
2013	623	2217	9.5	9.964	-85.664	21	4	0.1	0.8CUNA
2013	623	2221	25.6	10.074	-85.696	0.1	3	0.1	0.5CUNA
2013	623	2231	23.4	10.036	-85.671	0.2	3	0.5	0.5CUNA
2013	623	2233	56.1	9.968	-85.642	20	3	0	1.2CUNA
2013	623	2241	27.1	9.94	-85.657	20.8	3	0.1	1.2CUNA
2013	623	2305	52.1	9.943	-85.624	19.9	3	0	1.0CUNA
2013	623	2306	28.8	9.963	-85.615	20	3	0	0.9CUNA
2013	623	2314	5.6	9.938	-85.62	19.6	3	0	1.1CUNA
2013	623	2315	13.4	9.972	-85.612	19.2	3	0.1	0.7CUNA
2013	623	2327	11.3	10.09	-85.736	0	3	0.3	0.3CUNA
2013	623	2348	29.1	9.939	-85.618	15.3	3	0.5	0.7CUNA
2013	624	1	17	9.978	-85.627	19.5	3	0	1.0CUNA

2013	624	2	21.4	10.217	-85.851	17.1	3	2.4	0.9CUNA
2013	624	26	47.3	9.934	-85.618	20	3	0.1	0.6CUNA
2013	624	38	4	9.995	-85.554	21.4	3	0	0.9CUNA
2013	624	44	48.6	9.973	-85.627	20.2	4	0	1.2CUNA
2013	624	56	18.7	9.932	-85.63	21	3	0	1.0CUNA
2013	624	123	48	9.955	-85.64	20.9	3	0	0.8CUNA
2013	624	127	19.1	9.969	-85.641	20.5	3	0	0.7CUNA
2013	624	154	27.5	9.979	-85.627	19.5	4	0	0.7CUNA
2013	624	155	26.1	9.945	-85.629	20.1	3	0	0.9CUNA
2013	624	226	27.6	9.952	-85.632	20.3	3	0	0.7CUNA
2013	624	302	22.3	9.928	-85.677	21.3	4	0.3	1.2CUNA
2013	624	317	40.8	10.121	-85.5	14.2	4	1.4	0.7CUNA
2013	624	425	30.1	9.937	-85.616	20.6	4	0.1	0.8CUNA
2013	624	515	46.3	9.916	-85.611	20.2	3	0.1	1.1CUNA
2013	624	644	42.7	9.954	-85.634	21	3	0	1.2CUNA
2013	624	735	23.2	10.035	-85.374	3.7	3	2.3	1.3CUNA
2013	624	841	26	9.963	-85.641	20.4	3	0	1.1CUNA
2013	624	1358	47.8	9.929	-85.619	21	3	0.1	1.3CUNA
2013	624	1516	10	9.944	-85.586	22.6	3	0.2	0.7CUNA
2013	624	1537	19.4	9.933	-85.604	19.8	4	0.1	1.1CUNA
2013	624	1735	40	9.946	-85.62	20.3	3	0	1.1CUNA
2013	624	1837	48.1	9.954	-85.631	20.4	3	0	1.1CUNA
2013	624	1837	24.1	9.947	-85.577	21.6	5	0.4	1.1CUNA
2013	624	1921	18	9.938	-85.611	20	4	0.1	1.1CUNA
2013	625	611	34.2	9.921	-85.629	22	3	0.1	0.7CUNA
2013	625	1058	32	9.933	-85.625	19.8	3	0	1.0CUNA
2013	625	1755	1.3	9.826	-85.533	14.3	3	1.5	0.7CUNA
2013	625	1820	1.8	9.977	-85.591	20.8	3	0	0.8CUNA
2013	625	1955	7.9	9.945	-85.713	21.2	3	0.2	1.0CUNA
2013	626	711	29.8	10.089	-85.645	14.2	3	0.2	0.5CUNA
2013	626	1012	51	10.059	-85.694	0.1	3	0.1	0.5CUNA
2013	626	2021	17.5	10.429	-85.955	21.7	4	0.1	1.6CUNA
2013	626	2119	21.1	9.936	-85.748	19.2	4	0	1.2CUNA
2013	627	316	53.8	10.07	-85.629	22.7	3	0.3	0.5CUNA
2013	627	810	24.6	10.205	-85.978	21.1	3	0	1.3CUNA
2013	627	1027	37.9	10.08	-85.695	9.8	3	0.1	0.4CUNA
2013	627	1007	32	10.007	-85.646	19.2	3	0.1	0.4CUNA
2013	628	126	11.8	10.197	-85.526	22.2	4	0.2	0.9CUNA
2013	628	956	18.8	9.99	-85.654	19.8	3	0.1	0.6CUNA
2013	628	1458	39.9	9.942	-85.63	19.7	3	0	0.5CUNA
2013	628	2144	44.8	9.947	-85.624	18.9	5	0.2	0.8CUNA
2013	629	30	41.5	9.878	-85.61	18.3	4	0.1	0.4CUNA
2013	629	438	38.6	9.848	-85.617	18.6	3	0.1	0.7CUNA

2013	629	505	9.1	10.199	-85.612	20	3	0	1CUNA
2013	629	834	48	9.84	-85.581	18.5	3	0	0.6CUNA
2013	629	942	16.6	9.868	-85.676	16	3	0.2	0.4CUNA
2013	629	1240	53.8	10.527	-84.892	20	3	0.7	2.5CUNA
2013	629	1946	32.8	9.972	-85.65	18.8	5	0.2	1.0CUNA
2013	630	449	8.8	9.9	-85.552	9.8	3	0.2	0.1CUNA
2013	630	547	32.2	9.856	-85.644	14.8	4	0.5	1.1CUNA
2013	630	906	37.9	10.382	-85.491	37.3	4	0.1	1.5CUNA
2013	630	1944	59.2	10.22	-85.707	28.2	4	0.3	0.8CUNA
2013	701	332	13.5	10.164	-84.853	20	6	4.3	1.0CUNA
2013	701	450	52.1	9.978	-85.36	20.4	3	0.1	0.8CUNA
2013	701	421	3.1	10.072	-85.709	0.6	3	0.2	0.0CUNA
2013	701	548	6.8	10.255	-84.89	40	5	2.6	2.1CUNA
2013	701	615	18.7	10.001	-84.854	42	4	4.4	1.0CUNA
2013	701	802	25.9	9.931	-85.345	19	3	0	0.8CUNA
2013	701	805	31.3	9.951	-84.901	29.7	4	2.8	1.4CUNA
2013	701	903	5.4	9.912	-85.355	20.5	3	0.1	0.9CUNA
2013	701	918	53	9.92	-85.328	18.9	3	0.1	1.1CUNA
2013	701	940	58.7	10.045	-84.858	33.1	5	4.1	1.6CUNA
2013	701	2342	26.1	9.997	-85.081	38.8	4	3.2	0.7CUNA
2013	702	54	50.5	9.978	-84.913	61.1	5	0.2	1.5CUNA
2013	702	242	1.9	9.945	-85.362	17.9	4	0.1	1.1CUNA
2013	702	1153	40	9.622	-87.417	20	3	0.6	2.9CUNA
2013	702	1712	19.1	11.886	-86.406	20	5	1.2	2.9CUNA
2013	703	20	50.4	9.869	-85.505	17.2	3	0	0.8CUNA
2013	703	356	53.6	9.824	-85.603	15.7	3	0	0.3CUNA
2013	703	555	57.6	9.891	-85.626	16.1	3	0.2	0.4CUNA
2013	703	530	58.4	11.189	-87.021	20	3	0.4	2.8CUNA
2013	703	612	34.7	9.961	-85.661	18.6	4	0.1	0.7CUNA
2013	703	903	15.2	9.963	-85.659	19.9	4	0.1	0.7CUNA
2013	703	1010	40.3	11.35	-85.539	20	4	0.6	2.7CUNA
2013	703	1111	4.8	9.941	-85.634	21.2	4	0	0.5CUNA
2013	703	1205	52.3	9.972	-85.654	19.3	4	0	0.7CUNA
2013	703	1301	2.4	9.84	-85.604	17.8	4	0.1	0.6CUNA
2013	703	1441	24.2	9.949	-85.64	20.3	6	0.1	1.1CUNA
2013	703	1529	38.4	9.839	-85.602	17.9	4	0.1	0.8CUNA
2013	703	1630	37.8	9.92	-85.761	19.2	3	0	1.2CUNA
2013	703	2119	14.4	9.84	-85.603	17.7	4	0.1	0.7CUNA
2013	703	2315	49.4	9.625	-85.173	12.7	4	0.2	1.6CUNA
2013	704	24	39.3	9.839	-85.565	18	7	0.1	0.7CUNA
2013	704	204	12.4	9.834	-85.617	17.2	3	0	0.4CUNA
2013	704	215	11.3	9.917	-85.302	18	8	0.1	1.3CUNA
2013	704	522	11.1	10.46	-84.25	89.9	4	0.3	2.6CUNA

2013	704	600	50	9.833	-85.614	17.5	3	0.1	0.6CUNA
2013	704	605	27.9	9.845	-85.6	18.5	4	0.1	0.6CUNA
2013	704	606	41.4	9.848	-85.611	17.6	4	0	0.3CUNA
2013	704	607	56.5	9.866	-85.605	17.8	3	0	0.1CUNA
2013	704	636	41.8	9.901	-85.598	20	3	0.1	0.3CUNA
2013	704	758	55.7	10.043	-85.735	15	4	0.6	0.3CUNA
2013	704	706	37.2	9.915	-84.469	90	7	0.4	2.3CUNA
2013	704	813	51.1	9.927	-85.635	15.6	4	0.2	0.2CUNA
2013	704	1007	19.7	9.828	-85.619	17	4	0.1	0.4CUNA
2013	704	1028	19.8	9.749	-85.803	22.4	8	0.1	1.8CUNA
2013	704	1222	55.1	9.892	-85.337	20.9	4	0.1	1.2CUNA
2013	704	1308	38	10.415	-85.191	86.1	4	0	2.0CUNA
2013	704	1322	22.6	10.065	-85.879	22.7	3	0.3	0.7CUNA
2013	704	1355	25.8	9.854	-85.426	14.1	3	0.1	0.4CUNA
2013	704	1455	7.7	9.774	-85.707	5.7	3	0.1	1.2CUNA
2013	704	1531	12.5	9.981	-85.632	18.2	3	0	0.5CUNA
2013	704	1504	11.8	9.705	-85.796	20	3	0.2	1.9CUNA
2013	704	1651	45.7	9.988	-85.66	23.6	4	0	0.8CUNA
2013	704	2125	6.7	9.781	-85.644	20	3	0.2	1.0CUNA
2013	704	2124	16.3	9.973	-85.344	5.2	3	0	0.8CUNA
2013	704	2232	6	9.848	-85.621	18.1	5	0.1	0.4CUNA
2013	705	509	15.9	9.821	-85.585	25.9	4	0	0.6CUNA
2013	705	538	0.5	9.968	-85.657	19.7	4	0.1	0.4CUNA
2013	705	1039	31.2	9.843	-84.051	14.8	5	0.3	2.7CUNA
2013	705	1317	52.2	9.962	-85.611	20.2	5	0.5	1.4CUNA
2013	705	1540	58.9	9.867	-86.056	0.6	3	1.4	1.0CUNA
2013	705	1709	42.9	9.968	-85.636	35.5	3	0.5	0.9CUNA
2013	705	1817	3.2	9.945	-85.755	5.2	4	0.2	0.6CUNA
2013	705	1923	33.6	9.888	-84.98	20	3	0.1	1.7CUNA
2013	706	51	19.1	9.589	-84.901	9.4	4	0.3	1.7CUNA
2013	706	542	56.9	9.962	-85.638	19.7	5	0	0.5CUNA
2013	706	1219	41.9	9.94	-85.621	18.1	3	0	0.3CUNA
2013	707	251	19.3	10.165	-85.668	20	9	0	1
2013	707	400	58.9	9.892	-85.052	64.7	5	0.3	1.8CUNA
2013	707	600	11.3	11.23	-86.536	20	4	0.6	2.7CUNA
2013	707	744	12.3	10.015	-85.653	20.2	3	0	0.5CUNA
2013	707	914	28.7	10.02	-85.654	20.7	4	0.1	0.6CUNA
2013	707	1515	23.2	10.204	-85.732	22.8	6	0.3	0.8CUNA
2013	708	654	26.5	10.19	-85.689	22.8	5	0.3	1.0CUNA
2013	708	609	0.3	9.945	-85.55	22.7	5	0.1	0.4CUNA
2013	708	732	48.3	9.975	-85.66	19.8	4	0.1	1.0CUNA
2013	708	912	59.7	10.977	-84.407	12.1	4	0.5	2.5CUNA
2013	708	1014	1.4	10.96	-87.057	19.7	3	0.4	2.6CUNA

2013	708	2111	39.4	10.087	-85.769	0.1	5	0.4	0.5CUNA
2013	709	11	15.4	9.645	-84.176	22.4	9	0.3	2.7CUNA
2013	709	108	43.5	9.459	-84.188	23.5	4	0.3	2.2CUNA
2013	709	202	1.2	9.307	-85.953	55.3	4	0	1.5CUNA
2013	709	404	25	9.618	-85.119	5.1	4	0.5	1.5CUNA
2013	709	547	29.6	9.953	-85.659	17.8	3	0.1	0.4CUNA
2013	709	806	40.9	9.958	-85.775	16.6	3	0	0.6CUNA
2013	709	820	3.3	9.622	-85.166	21.9	4	0.2	1.6CUNA
2013	709	1409	42	9.982	-85.722	11.2	4	0.6	0.3CUNA
2013	709	1510	58.5	10.161	-85.725	26.8	5	0.9	1.0CUNA
2013	710	212	57.6	9.816	-85.515	21.2	4	0.3	0.5CUNA
2013	710	346	14.7	10.122	-85.576	13.7	3	0.1	0.9CUNA
2013	710	651	47.5	9.913	-85.459	0.4	5	0.3	1
2013	710	733	59	10.157	-85.709	25.3	6	0.1	0.9CUNA
2013	710	1112	54.2	9.966	-85.643	15.2	4	0.8	0.5CUNA
2013	710	1228	54.4	10.516	-86.278	29.7	7	0.2	2.7CUNA
2013	710	1335	51.1	9.966	-85.641	19.8	4	0	0.5CUNA
2013	710	1831	23.1	10.173	-85.717	22.7	5	0.1	1.3CUNA
2013	710	1939	46.8	9.867	-85.464	27.1	3	0	0.7CUNA
2013	711	517	22.8	9.803	-85.551	16.9	3	0	0.5CUNA
2013	711	539	50	10.018	-85.657	19.8	5	0.1	0.7CUNA
2013	711	847	16.5	10.169	-85.712	23.3	6	0.1	1.3CUNA
2013	711	1133	47.5	9.816	-85.599	16.4	3	0	1
2013	711	1142	6	10.054	-85.541	3.2	4	0.5	0.3CUNA
2013	711	1655	13.9	10.299	-85.612	8.5	4	1.4	1.2CUNA
2013	711	1749	54.6	9.893	-85.246	26.2	4	0.3	1.5CUNA
2013	711	1800	36.1	9.958	-85.649	18.9	6	0.2	1.1CUNA
2013	711	2152	46.4	10.041	-85.872	4.7	3	0.3	0.8CUNA
2013	711	2357	11.1	9.951	-85.675	16.6	5	0.1	0.7CUNA
2013	712	109	55.3	9.858	-85.615	17.7	4	0.1	0.5CUNA
2013	712	602	19.1	9.956	-85.759	20	3	0.2	0.7CUNA
2013	712	1006	23.2	9.952	-85.777	16	3	0	0.8CUNA
2013	712	1109	10	9.873	-85.318	5.2	3	0.1	0.9CUNA
2013	712	1712	3.2	10.172	-85.983	18.4	5	0.1	1.3CUNA
2013	713	544	26.5	9.825	-85.644	31.8	3	0.5	1.1CUNA
2013	713	630	12.2	9.944	-85.637	21.8	3	0.5	1.0CUNA
2013	713	1202	21.7	10.208	-85.992	5.2	3	0	1.6CUNA
2013	713	1309	59	10	-85.459	30.1	3	0	0.8CUNA
2013	713	1447	16.9	10.06	-85.63	14.7	3	0.3	0.5CUNA
2013	713	2038	56.5	10.27	-85.788	36.3	4	0.3	1.4CUNA
2013	713	2241	18.9	10.723	-85.799	52.3	7	0.7	2.2CUNA
2013	714	141	38.8	9.816	-85.609	15.2	3	0.1	0.4CUNA
2013	714	349	50.2	9.676	-85.336	18.7	3	0.2	1.3CUNA

2013	714	426	24.7	9.995	-85.673	15.5	3	0.1	0.5CUNA
2013	714	415	6.1	9.983	-85.68	17.4	4	0	1.0CUNA
2013	714	1011	12.5	9.953	-85.66	20	3	0.1	0.4CUNA
2013	714	1242	53.2	10.027	-85.689	20.7	4	0	1.1CUNA
2013	714	1342	28.9	9.96	-85.66	17.7	5	0.1	0.7CUNA
2013	714	1651	2.1	9.957	-85.552	20.3	5	0.1	0.9CUNA
2013	714	1948	22.1	9.829	-85.56	17.4	4	0	0.8CUNA
2013	714	2000	52.9	9.968	-85.335	24.8	3	0	1.2CUNA
2013	715	310	16	9.917	-85.602	32.9	3	0.3	0.8CUNA
2013	715	838	19.9	9.943	-85.776	16.5	3	0.1	0.8CUNA
2013	715	1008	53.5	10.026	-85.669	19	4	0	0.5CUNA
2013	715	1150	17.5	9.95	-85.509	27	3	0.1	0.8CUNA
2013	715	1831	29.5	10.182	-85.413	61.6	3	0.1	1.8CUNA
2013	715	2131	43.2	9.889	-85.435	16.9	3	0	0.6CUNA
2013	716	216	1.4	9.619	-85.881	29.5	3	0.1	1.5CUNA
2013	716	217	32.7	9.845	-85.362	19.7	4	0	1.0CUNA
2013	716	255	40.6	9.805	-85.602	12.9	3	0.1	0.3CUNA
2013	716	317	14.4	9.802	-85.568	16.3	3	0.1	1.1CUNA
2013	716	421	27.6	9.873	-85.654	17.4	3	0	0.6CUNA
2013	716	545	29	10.119	-85.531	20	3	0	1.0CUNA
2013	716	643	6	9.95	-85.646	17	3	0	0.5CUNA
2013	716	903	5.8	9.42	-85.636	5.2	3	0.1	1.3CUNA
2013	716	1024	12.6	10.667	-85.452	89.8	4	0.1	2.4CUNA
2013	716	1848	19.1	9.979	-85.684	18.7	3	0	0.7CUNA
2013	716	2038	27.6	9.847	-85.42	21.7	3	0	1.2CUNA
2013	717	139	31.7	9.953	-85.663	18.4	4	0.1	0.7CUNA
2013	717	351	49.5	9.971	-85.654	17.5	5	0.1	0.4CUNA
2013	717	513	51.7	9.992	-85.692	16.2	3	0	0.4CUNA
2013	717	600	26.7	9.958	-85.687	20	3	0.2	0.5CUNA
2013	717	720	44.9	10.248	-85.796	5.1	3	0.1	1.0CUNA
2013	717	738	8.2	10.084	-85.662	25.4	3	0	0.8CUNA
2013	717	1412	5.6	9.954	-85.665	19.1	3	0	0.5CUNA
2013	718	443	1.7	10.515	-84.678	20	4	0.4	2.2CUNA
2013	718	754	48.3	9.945	-85.645	17.9	3	0.1	0.5CUNA
2013	718	726	17	9.977	-85.7	18.3	3	0	0.4CUNA
2013	718	841	40.2	10.049	-85.639	29.3	3	0	0.7CUNA
2013	718	949	8.8	9.943	-85.66	27.5	4	0.2	0.7CUNA
2013	718	1407	26.5	10.066	-85.643	25.9	3	0	0.8CUNA
2013	718	1406	10	10.087	-85.659	22.3	5	0	1.2CUNA
2013	718	1407	7.9	10.05	-85.646	26.1	3	0	0.8CUNA
2013	718	1520	4	9.944	-85.647	18.9	3	0	0.6CUNA

Table 1: List of all earthquakes with the time of the event's first arrival, the latitude and longitude, the depth, the number of polarities picked, the RMS value, and the coda magnitude.